NASA TECHNICAL NOTE

NASA TN D-6084

STUDY OF TURBOJET COMBUSTOR DYNAMICS USING SWEEP-FREQUENCY DATA

by John R. Szuch, Francis J. Paulovich, and William M. Bruton

Lewis Research Center
Cleveland, Ohio 44135

NATIONAL AERONAUTICS AND SPACE ADMINISTRATION • WASHINGTON, D. C. • NOVEMBER 1970

1. Report No.	2. Government Accession No.	3. Recip
NASA TN D-6084		

4. Title and Subtitle
STUDY OF TURBOJET COMBUSTOR DYNAMICS USING SWEEP-FREQUENCY DATA

5. Report Date
November 1970

6. Performing Organization Code

7. Author(s)
John R. Szuch, Francis J. Paulovich, and William M. Bruton

8. Performing Organization Report No.
E-5595

10. Work Unit No.
720-03

9. Performing Organization Name and Address
Lewis Research Center
National Aeronautics and Space Administration
Cleveland, Ohio 44135

11. Contract or Grant No.

13. Type of Report and Period Covered
Technical Note

12. Sponsoring Agency Name and Address
National Aeronautics and Space Administration
Washington, D. C. 20546

14. Sponsoring Agency Code

15. Supplementary Notes

16. Abstract

The analysis of data obtained from sweep-frequency testing of the J85 turbojet combustor is discussed. Bode plots of the response of combustor pressure to sinusoidal disturbances in fuel-spray-nozzle pressure are presented for a range of fuel flows. An analog simulation was developed and used to match the experimental data and to identify the combustion dynamics. The effects of primary or burning-zone fuel-to-air ratio on the system response were also investigated. The experimental data were fit by linear transfer function forms to be used in overall system studies.

17. Key Words (Suggested by Author(s))
Turbojet; Combustor; Combustion; Dynamics; Analog; Simulation; Burning; Transfer function; J85; Dead time; Engine; Gas mixing; Time constant; Fuel-air ratio; Response

18. Distribution Statement
Unclassified - unlimited

19. Security Classif. (of this report)	20. Security Classif. (of this page)	21. No. of Pages	22. Price*
Unclassified	Unclassified	41	$3.00

*For sale by the Clearinghouse for Federal Scientific and Technical Information
Springfield, Virginia 22151

STUDY OF TURBOJET COMBUSTOR DYNAMICS USING SWEEP-FREQUENCY DATA

by John R. Szuch, Francis J. Paulovich, and William M. Bruton

Lewis Research Center

SUMMARY

Tests were conducted to determine the response of the J85 turbojet combustor pressure to sweep-frequency, sinusoidal oscillations in fuel-spray nozzle pressure. A Fourier analysis program was used to generate Bode plots of the response characteristics.

An analog computer simulation of the turbojet combustor was also developed. The simulation was used to determine the form of the fuel combustion dynamics required to match the experimental data. A dead time second-order lag combination for the fuel combustion dynamics was determined. The dead time was relatively insensitive to fuel flow, varying between 2.6 and 3.2 milliseconds. The second-order lag had a natural frequency of 55 hertz and a damping ratio that varied inversely with fuel flow, ranging from 0.7 to 0.5. The effect of fuel flow on damping ratio was attributed to the primary-combustion or burning zone expanding toward the combustor-pressure measuring station. The effects of the burning-zone mixture ratio on the response were also determined using the simulation. For fixed flows to the combustor, the zero-frequency amplitude ratio for the response was a strong function of the burning-zone mixture ratio.

Transfer functions, obtained from curve fitting the Bode plots of the experimental data, were also determined. The response of the combustor pressure to fuel-spray nozzle pressure could be represented by a dead time first-order-lag, second-order-lag combination. The dead time was equal to the simulation value for all but the highest fuel flow rate case. The first-order lag was related to the mixing of combustion products and airflow in the secondary-combustion or mixing zone. The second-order lag had a natural frequency of 55 hertz, indicating that the simulated fuel-combustion process dominates the closed-loop response that was fit. The damping ratio varied inversely with fuel flow, ranging from 0.9 to 0.7.

INTRODUCTION

The demand for rapid thrust changes in turbojet aircraft requires knowledge of the dynamic response of combustor pressure and temperature to disturbances in fuel flow. The rapid increase in turbine-inlet temperature must be accomplished while avoiding compressor stall, combustor blowout due to excessive fuel-to-air ratios, and excessive turbine-blade temperatures. In addition, the analysis of high-frequency interactions between engine and inlet dynamics requires an understanding of the combustion dynamics involved.

Evaluations of combustor response to fuel-flow disturbances have often been based on transient data. Reference 1 used step changes in fuel flow to study the time response of combustor-outlet temperature for comparison with analytical results. Results from that study indicated that the response was higher than first order. However, no attempt was made to identify the source of the dynamics. References 2 and 3 used similar test data to evaluate the effects of various injection methods on performance and blowout limits. Reference 4 used step changes in fuel flow to design and evaluate fuel-control systems.

One obvious limitation in trying to evaluate combustor dynamics using transient data is the difficulty in measuring small time delays of the order of a millisecond. Reference 5 reported results obtained from sinusoidal disturbances in fuel flow. However, no phase data were reported, so the observed dynamic response was attributed to lag effects rather than to time delays.

High-response electrohydraulic fuel controls were first developed by NACA in the 1950's (ref. 6) making the investigation reported in reference 5 possible. Significant improvements in these controls have been made in recent years and are reported in references 7 to 9. In addition, improved data analysis techniques have made it possible to automatically obtain frequency-response plots when fuel flow is varied sinusoidally with frequency being swept linearly or logarithmically. A Fourier analysis program (ref. 10) has been developed to reduce the sweep-frequency data yielding amplitude and phase information. Accurate phase data at high frequencies (about 100 Hz) allows determination of any time delays present in the combustor response.

Tests were conducted on an afterburning turbojet engine in the Lewis 10- by 10-Foot Supersonic Wind Tunnel. Fuel flow was supplied from a high-response electrohydraulic fuel valve commanded by a sweep-frequency generator. The Fourier analysis program (ref. 10) was implemented on an analog computer. The program yielded Bode plots of the response of the combustor pressure to sinusoidal oscillations in the fuel spray-nozzle pressure for a range of fuel flow rates.

For comparison with experimental data an analytical model was developed and implemented on the analog computer. The computer model assumed that the combustor con-

sisted of a primary-combustion or burning zone and a secondary-combustion or mixing zone. The fuel, together with a portion of the total airflow, was assumed to be completely burned in the burning zone. The remaining airflow was assumed to mix with the combustion products in the mixing zone. The model allowed variations in the burning-zone fuel to air ratio. In addition, fuel combustion dynamics could be introduced in the model to match the experimental results.

Transfer functions, obtained from curve-fitting the experimental data, were also determined. This information should prove useful in overall system studies where reimplementation of the entire analog simulation might be undesirable.

APPARATUS AND PROCEDURE

A cutaway view of the engine and inlet is shown in figure 1. The engine, a General Electric Company model J85-13, is a single-rotor afterburning turbojet engine with an eight-stage compressor, an annular combustor, and a two-stage turbine. The engine is equipped with a variable-area exhaust nozzle. The inlet is axisymmetric and has mixed-compression with 60 percent of the supersonic area contraction occurring internally at design Mach 2.5. The inlet cowl-lip diameter is 47.3 centimeters, corresponding to a capture flow area of 1760 square centimeters. For this study, only the nonafterburning mode of operation was used. For all tests, the average free-stream Mach number in the wind tunnel was 2.5 with the inlet-engine system operated at a zero angle of attack. Table I(a) summarizes the test conditions for this study. Fuel flows, ranging from .0517 to 0.132 kilogram per second, were run with corrected speeds ranging from 83.1 to 88.3 percent of the design value.

Figure 2 is a cutaway view of the combustor section. Commercial jet fuel was supplied to the combustor from a high-response electrohydraulic fuel valve commanded by a sweep-frequency generator. A description of the valve is found in reference 7. All the fuel was injected into the main combustor section by means of 12 equally space spray nozzles. A cutaway view of one of the nozzles and its flow divider is shown in figure 3. The initial flow of fuel passes through the primary tube to the primary-nozzle orifice where the spray pattern is formed for combustion. As the pressure across the nozzle increases above 82.7 newtons per square centimeter, a spring-loaded valve in the divider housing starts to open. This action allows flow through the secondary tube and orifice to supplement the fuel requirements. Reference 2 discusses the high performance obtained with this type of nozzle. Figure 4 shows a calibration curve for the 12 nozzles obtained from cold-flow testing of a single nozzle.

The pressure measurements of interest for this study were made in the spray-nozzle divider housing and in the outer combustor annulus (see fig. 2). Signals from these

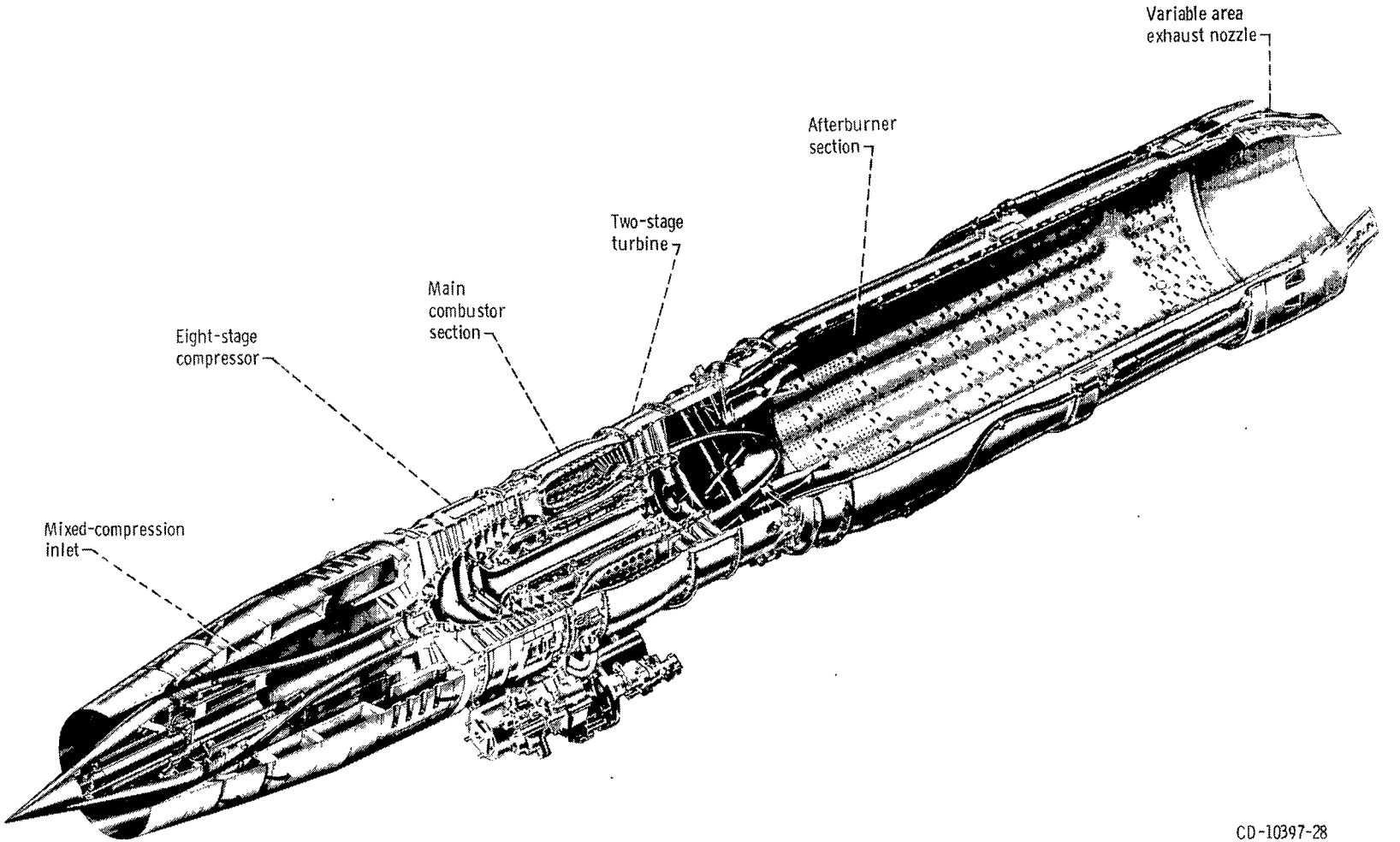

Figure 1. - Cutaway view of inlet engine used for supersonic wind tunnel tests.

TABLE I. - STEADY-STATE OPERATING CONDITIONS

(a) Test measurements

Test	Fuel flow, kg/sec	Percent corrected speed	Compressor pressure ratio	Total airflow, kg/sec	Compressor discharge		Combustor pressure, N/cm^2	Spray-nozzle pressure, N/cm^2
					Pressure, N/cm^2	Temperature, K		
A	0.052	86.3	3.77	12.6	30.4	460	28.5	112
B	.076	87.8	4.17	13.1	33.0	466	31.8	123
C	.092	87.4	4.19	12.9	34.0	479	32.2	128
D	.106	83.1	3.77	11.6	30.4	457	29.4	130
E	.132	88.2	4.63	12.9	37.0	485	35.4	144

(b) Simulation values at adjusted fuel-air ratio

Test	Burning-zone fuel-to-air ratio	Total airflow, kg/sec	Burning-zone airflow, kg/sec	Mixing-zone airflow, kg/sec	Bypass airflow, kg/sec	Burning zone			Mixing zone		
						Enthalpy, J/kg	Gas constant, J/kg	Specific heat, J/kg	Enthalpy, J/kg	Gas constant, J/kg	Specific heat, J/kg
A	0.0832	12.5	0.621	10.6	1.32	3.74×10^6	3.60×10^3	1.63×10^3	6.53×10^5	3.45×10^3	1.04×10^3
B	.0918	12.6	.830	10.5	1.33	3.41	3.67	1.55	6.97	3.45	1.05
C	.0932	12.6	.993	10.2	1.26	3.38	3.69	1.54	7.55	3.45	1.05
D	.0863	11.4	1.22	8.53	1.64	3.58	3.62	1.58	8.74	3.45	1.07
E	.0874	12.6	1.51	9.89	1.27	3.55	3.64	1.57	9.16	3.46	1.08

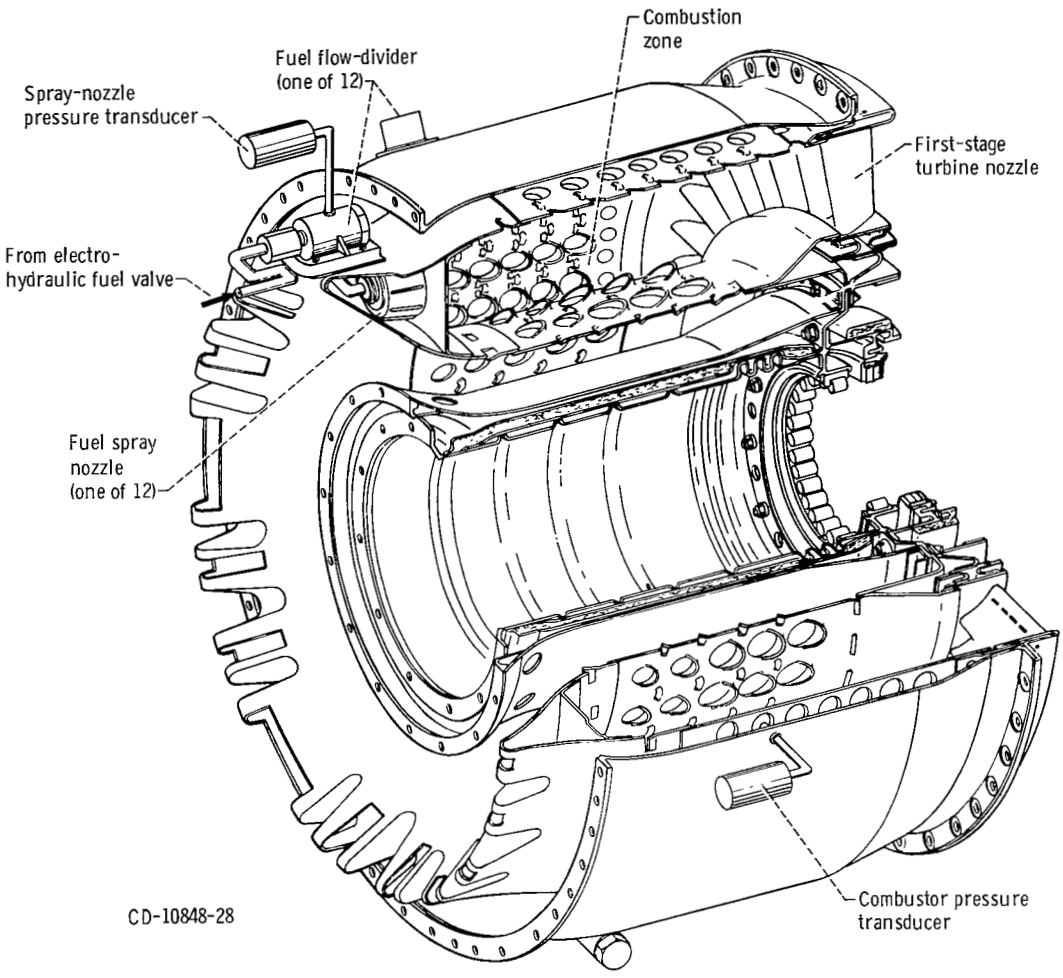

Figure 2. - Cutaway view of main combustor section.

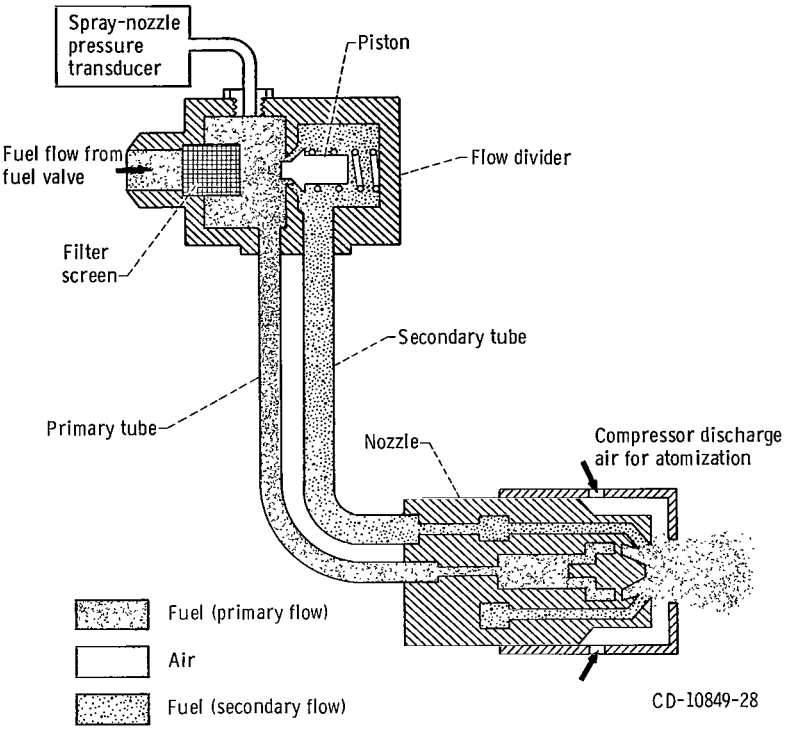

Figure 3. - Flow divider and spray nozzle.

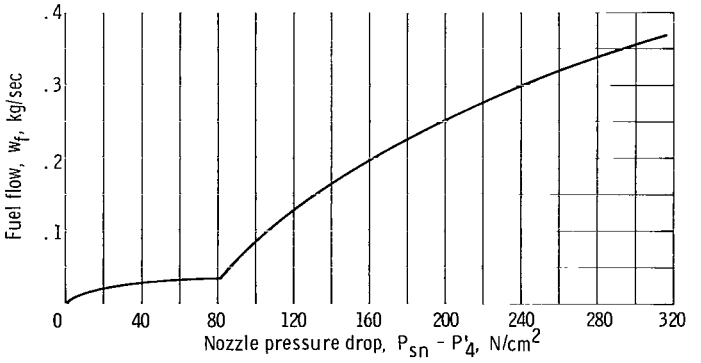

Figure 4. - Total fuel flow through 12 spray nozzles as function of spray-nozzle pressure drop (based on cold-flow tests of one nozzle).

transducers were recorded on magnetic tape together with the valve command signal.

A logarithmic sweep rate of 1 decade per minute was used with frequency ranging from 0.5 to 130 hertz. The frequency response of the fuel valve, when closely coupled to the combustor, is flat out to about 100 hertz. For these tests, however, the fuel valve was separated from the combustor by about 7 meters of both rigid and flexible lines. Resonances in fuel-flow, spray-nozzle pressure, and combustor pressure, which were caused by the line dynamics, were observed during the testing. To eliminate these effects from the data, the ratio of the response of combustor pressure to disturbances in fuel flow to the corresponding response of spray nozzle pressure was used. The strain-gage pressure transducers had flat frequency responses (±2 dB) out to about 120 hertz for the magnitude of the disturbances used in the test program.

A Fourier reduction program described in reference 10 was implemented on an analog computer. The program was used to determine the relation between the combustor-pressure oscillations and the spray-nozzle-pressure oscillations. Each previously recorded pressure signal was referenced to the fuel valve command signal to determine, as the frequency was varied, the real and imaginary parts of the corresponding transfer functions. This information was displayed on an x-y recorder to obtain the amplitude and phase angle for each pressure to command signal response. This procedure was repeated for each of the five selected tests. By forming amplitude ratios and subtracting the phase angles, the amplitude and phase angle of the combustor-pressure to spray-nozzle-pressure ratio transfer function were obtained for each test. A digital reduction program has recently been developed to generate the Bode plots directly. Where possible, analog-reduced data were compared with digitally reduced data.

EXPERIMENTAL RESULTS AND ANALYSIS

The following sections will present the results of the sweep-frequency testing for five selected tests. These tests cover a range of fuel flow rates from 0.0517 to 0.132 kilogram per second. The responses of combustor pressure to spray-nozzle pressure, obtained from the Fourier reduction program, are displayed as Bode plots.

To match the experimental data and to identify the source of the observed dynamics, an analog computer simulation was developed and will be described. Bode plots, obtained using the simulation, will be compared with experimental data.

Transfer functions, obtained from curve fitting of the experimental data will also be presented. This information should prove useful in overall system studies where re-implementation of the entire analog simulation might be undesirable.

TABLE II. - COMPARISON OF EXPERIMENTAL AND SIMULATION DATA FOR J85 COMBUSTOR TEST

(a) Test A; fuel flow rate, 0.052 kilogram per second

[Experimental data normalized at 12 Hz; simulation data normalized at 7 Hz.]

Experimental data								Simulation data			
Frequency, f, Hz	Spray-nozzle pressure, $\tilde{P}_{sn}$		Combustor pressure, $\tilde{P}_4$		Amplitude ratio, $\lvert\tilde{P}_4/\tilde{P}_{sn}\rvert$	Phase angle, $\angle\tilde{P}_4/\tilde{P}_{sn}$, deg	Normalized amplitude ratio, $\lvert\tilde{P}_4/\tilde{P}_{sn}\rvert/0.132$	Frequency, f, Hz	Amplitude ratio, $\lvert\tilde{P}_4/\tilde{P}_{sn}\rvert$	Phase angle, $\angle\tilde{P}_4/\tilde{P}_{sn}$, deg	Normalized amplitude ratio, $\lvert\tilde{P}_4/\tilde{P}_{sn}\rvert/0.132$
	Amplitude, N/cm^2	Phase, deg	Amplitude, N/cm^2	Phase, deg							
7	2.74	-50	0.374	-76	0.136	-26	1.03	7	0.132	-24	1.00
12	3.05	-80	.402	-119	.132	-39	1.00	10	.130	-34	.985
17	3.01	-122	.370	-176	.123	-54	.932	15	.125	-51	.947
22	2.22	-154	.272	-223	.123	-69	.932	20	.119	-66	.902
26	2.28	-175	.258	-256	.113	-81	.856	25	.111	-82	.841
30	2.26	-205	.238	-297	.105	-92	.795	30	.104	-98	.788
34	2.33	-234	.247	-334	.106	-100	.803	35	.0957	-114	.725
38	2.33	-265	.238	-379	.102	-114	.773	40	.0870	-128	.659
42	2.05	-307	.192	-429	.0933	-122	.707				
46	1.37	-344	.112	-475	.0819	-131	.620	45	.0782	-144	.592
51	.793	-370	.0658	-512	.0830	-142	.629	50	.0696	-158	.527
56	.534	-386	.0292	-533	.0547	-147	.414	60	.0565	-185	.428
74	.241	-412	.0110	-615	.0454	-203	.344	70	.0464	-209	.352
78	.225	-432	-----	----	-----	----	----	80	.0368	-232	.279
82	.192	-445	-----	----	-----	----	----	---	-----	----	----
86	.165	-452	-----	----	-----	----	----	---	-----	----	----
90	.145	-458	-----	----	-----	----	----	90	.0292	-253	.221
94	.143	-461	-----	-740	-----	-279	----	---	-----	----	----
98	.143	-466	-----	-740	-----	-274	----	100	.0233	-271	.176

(b) Test B; fuel flow rate, 0.076 kilogram per second

Experimental data								Simulation data			
Frequency, f, Hz	Spray-nozzle pressure, $\tilde{P}_{sn}$		Combustor pressure, $\tilde{P}_4$		Amplitude ratio, $\lvert\tilde{P}_4/\tilde{P}_{sn}\rvert$	Phase angle, $\angle\tilde{P}_4/\tilde{P}_{sn}$, deg	Normalized amplitude ratio, $\lvert\tilde{P}_4/\tilde{P}_{sn}\rvert/0.158$	Frequency, f, Hz	Amplitude ratio, $\lvert\tilde{P}_4/\tilde{P}_{sn}\rvert$	Phase angle, $\angle\tilde{P}_4/\tilde{P}_{sn}$, deg	Normalized amplitude ratio, $\lvert\tilde{P}_4/\tilde{P}_{sn}\rvert/0.196$
	Amplitude, $N\ cm^2$	Phase, deg	Amplitude, N/cm^2	Phase, deg							
7	6.03	-34	0.952	-64	0.158	-30	1.00	7	0.146	-25	1.00
12	7.65	-62	1.21	-106	.158	-44	1.00	10	.144	-36	986
17	10.0	-116	1.46	-172	.146	-56	.924	15	.137	-53	.938
22	5.48	-148	.752	-226	.137	-78	.867	20	.130	-70	.890
26	5.34	-176	.731	-269	.137	-93	.867	25	.120	-86	.822
30	4.77	-199	.614	-306	.129	-107	.816	30	.113	-102	.774
34	4.52	-220	.545	-341	.120	-121	.759	35	.104	-118	.712
38	4.52	-248	.530	-380	.117	-132	.740	40	.0956	-134	.655
42	4.11	-282	.457	-426	.111	-144	.702	---	-----	----	----
46	3.01	-316	.300	-472	.0995	-156	.630	45	.0871	-149	.596
51	1.97	-340	.165	-512	.0836	-172	.529	50	.0776	-164	.531
56	1.37	-354	.104	-541	.0759	-187	.480	60	.0631	-192	.432
69	.658	-368	.0421	-587	.0639	-219	.404	70	.0502	-218	.344
74	.814	-381	.0457	-606	.0562	-225	.356	---	-----	----	----
78	.724	-397	.0432	-621	.0596	-224	.377	80	.0393	-242	.269
82	.647	-409	.0208	-647	.0322	-238	.204	---	-----	----	----
86	.603	-416	.0175	-692	.0290	-276	.184	---	-----	----	----
90	.603	-422	.0183	-690	.0303	-268	.192	90	.0309	-263	.212
--	----	----	-----	----	-----	----	----	100	.0240	-283	.164

TABLE II. - Continued. COMPARISON OF EXPERIMENTAL AND SIMULATION DATA FOR J85 COMBUSTOR TEST

(c) Test C; fuel flow rate, 0.092 kilogram per second

[Experimental data normalized at 12 Hz; simulation data normalized at 7 Hz.]

Experimental data								Simulation data			
Frequency, f, Hz	Spray-nozzle pressure, $\tilde{P}_{sn}$		Combustor pressure, $\tilde{P}_4$		Amplitude ratio, $\lvert\tilde{P}_4/\tilde{P}_{sn}\rvert$	Phase angle, $\angle\tilde{P}_4/\tilde{P}_{sn}$, deg	Normalized amplitude ratio, $\lvert\tilde{P}_4/\tilde{P}_{sn}\rvert/0.126$	Frequency, f, Hz	Amplitude ratio, $\lvert\tilde{P}_4/\tilde{P}_{sn}\rvert$	Phase angle, $\angle\tilde{P}_4/\tilde{P}_{sn}$, deg	Normalized amplitude ratio, $\lvert\tilde{P}_4/\tilde{P}_{sn}\rvert/0.126$
	Amplitude, N/cm^2	Phase, deg	Amplitude, N/cm^2	Phase, deg							
7	4.38	-50	0.548	-80	0.125	-30	0.992	7	0.126	-25	1.00
12	4.80	-82	.603	-127	.126	-45	1.00	10	.124	-35	.984
17	4.94	-119	.567	-182	.115	-63	.913	15	.119	-52	.944
22	4.11	-147	.438	-230	.107	-83	.849	20	.114	-69	.905
26	4.11	-177	.430	-275	.104	-98	.825	25	.106	-86	.841
30	3.92	-204	.384	-315	.0979	-111	.777	30	.100	-102	.794
34	3.70	-232	.353	-354	.0953	-122	.756	35	.0930	-118	.738
38	3.54	-261	.311	-394	.0879	-133	.698	40	.0856	-134	.679
42	3.01	-292	.249	-434	.0826	-142	.656	--	-----	----	----
46	2.19	-322	.146	-475	.0667	-153	.529	45	.0779	-149	.618
51	1.51	-345	.0731	-513	.0484	-168	.384	50	.0697	-165	.553
--	----	----	-----	----	-----	----	----	60	.0563	-193	.447
78	.559	-416	-----	-640	-----	-224	----	70	.0445	-220	.353
82	.521	-428	-----	-680	-----	-252	----	80	.0344	-244	.273
86	.510	-437	-----	-694	-----	-257	----	--	-----	----	----
90	.521	-447	-----	-722	-----	-275	----	90	.0267	-266	.212
94	.548	-456	-----	-718	-----	-262	----	--	-----	----	----
--	----	----	-----	----	-----	----	----	100	.0206	-286	.163

(d) Test D; fuel flow rate, 0.106 kilogram per second

Experimental data								Simulation data			
Frequency, f, Hz	Spray-nozzle pressure, $\tilde{P}_{sn}$		Combustor pressure, $\tilde{P}_4$		Amplitude ratio, $\lvert\tilde{P}_4/\tilde{P}_{sn}\rvert$	Phase angle, $\angle\tilde{P}_4/\tilde{P}_{sn}$, deg	Normalized amplitude ratio, $\lvert\tilde{P}_4/\tilde{P}_{sn}\rvert/0.146$	Frequency, f, Hz	Amplitude ratio, $\lvert\tilde{P}_4/\tilde{P}_{sn}\rvert$	Phase angle, $\angle\tilde{P}_4/\tilde{P}_{sn}$, deg	Normalized amplitude ratio, $\lvert\tilde{P}_4/\tilde{P}_{sn}\rvert/0.172$
	Amplitude, N/cm^2	Phase, deg	Amplitude, N/cm^2	Phase, deg							
7	4.52	-36	0.640	-65	0.141	-29	0.966	7	0.172	-24	1.00
12	5.51	-64	.807	-104	.146	-40	1.00	10	.168	-33	.975
17	6.16	-108	.862	-161	.140	-53	.959	15	.161	-48	.933
22	4.72	-136	.614	-207	.130	-71	.890	20	.155	-64	.900
26	4.99	-168	.658	-253	.132	-85	.904	25	.149	-79	.867
30	4.38	-196	.556	-293	.127	-97	.870	30	.143	-94	.833
34	3.98	-221	.486	-330	.122	-106	.835	35	.136	-111	.792
38	3.62	-245	.411	-368	.114	-123	.781	40	.128	-127	.742
42	3.23	-273	.354	-407	.110	-134	.753	--	----	----	----
46	2.58	-302	.259	-448	.100	-146	.685	45	.117	-144	.679
51	1.92	-328	.177	-484	.0924	-156	.633	50	.106	-160	.614
56	1.40	-348	.113	-521	.0808	-173	.553	60	.0868	-191	.504
69	.685	-364	.0438	-583	.0640	-219	.438	70	.0688	-220	.400
74	.820	-380	.0450	-600	.0548	-220	.375	--	-----	----	----
78	.917	-400	.0391	-625	.0426	-225	.292	80	.0533	-246	.310
82	.685	-411	.0285	-635	.0416	-224	.285	--	-----	----	----
86	.658	-418	.0238	-644	.0362	-226	.248	--	-----	----	----
90	.658	-426	.0201	-695	.0306	-269	.210	90	.0414	-270	.241
--	----	----	-----	----	-----	----	----	100	.0323	-291	.187

TABLE II. - Concluded. COMPARISON OF EXPERIMENTAL AND SIMULATION DATA FOR J85 COMBUSTOR TEST

(e) Test E; fuel flow rate, 0.132 kilogram per second

Experimental data								Simulation data			
Frequency, f, Hz	Spray-nozzle pressure, $\tilde{P}_{sn}$		Combustor pressure, $\tilde{P}_4$		Amplitude ratio, $\lvert\tilde{P}_4/\tilde{P}_{sn}\rvert$	Phase angle, $\angle\tilde{P}_4/\tilde{P}_{sn}$, deg	Normalized amplitude ratio, $\lvert\tilde{P}_4/\tilde{P}_{sn}\rvert/0.147$	Frequency, f, Hz	Amplitude ratio, $\lvert\tilde{P}_4/\tilde{P}_{sn}\rvert$	Phase angle, $\angle\tilde{P}_4/\tilde{P}_{sn}$, deg	Normalized amplitude ratio, $\lvert\tilde{P}_4/\tilde{P}_{sn}\rvert/0.146$
	Amplitude, N/cm^2	Phase, deg	Amplitude, N/cm^2	Phase, deg							
7	10.1	-31	1.43	-57	0.142	-26	0.966	7	0.146	-21	1.00
12	11.6	-59	1.71	-96	.147	-37	1.00	10	.144	-30	.986
17	13.4	-101	1.92	-146	.143	-45	.973	15	.141	-44	.966
22	11.6	-129	1.60	-190	.137	-61	.932	20	.140	-59	.959
26	12.0	-165	1.66	-239	.138	-74	.939	25	.138	-74	.945
30	10.5	-194	1.46	-280	.139	-86	.946	30	.135	-89	.925
34	8.89	-219	1.28	-315	.144	-96	.980	35	.131	-105	.897
38	7.79	-243	1.03	-352	.133	-109	.905	40	.125	-122	.856
42	6.78	-266	.807	-388	.119	-122	.810	--	----	----	----
46	5.62	-288	.621	-422	.111	-134	.755	45	.116	-138	.794
51	4.45	-311	.475	-455	.107	-144	.728	50	.106	-154	.726
56	3.50	-331	.365	-486	.104	-155	.708	60	.0865	-185	.592
74	2.10	-370	.168	-595	.0803	-225	.546	70	.0680	-214	.466
78	2.10	-389	.148	-616	.0707	-227	.481	80	.0507	-239	.347
82	1.92	-402	.130	-635	.0676	-233	.460	--	-----	----	----
86	1.81	-412	.118	-655	.0656	-243	.446	--	-----	----	----
90	1.78	-418	.118	-675	.0667	-256	.454	90	.0375	-261	.257
--	----	----	----	----	-----	----	----	100	.0279	-280	.191

Experimental Data

Table II contains the pertinent information obtained from the Fourier analysis of tests A to E. Information beyond about 100 hertz was unintelligible because of low signal-to-noise ratios. In addition, data around 60 hertz were obscured by high noise levels.

Figures 5 to 9 contain the resultant plots of amplitude and phase for the ratio of combustor pressure to fuel spray-nozzle pressure. Also shown on figure 6 are the results from the digital reduction program. All data were normalized to an amplitude ratio of 1.0 at 12 hertz to eliminate any effects that rotor dynamics might have on the data.

Similar response characteristics were obtained for all runs. A slower fall-off in amplitude was observed for the tests having higher fuel flow rates (tests D and E, figs. 8 and 9). The slower fall-off could be attributed to the burning zone expanding downstream with the increase in fuel flow. An analysis, described in the following section, indicates that the burning zone expanded to include about 36 percent of the combustor volume for tests D and E. For these tests, the combustor-pressure transducer (fig. 2) would be less affected by combustor flow and mixing dynamics. A similar phenomenon was reported in reference 5 with slower fall-offs in turbine discharge temperatures attributed to burning in the tailpipe for locally high fuel-to-air ratios.

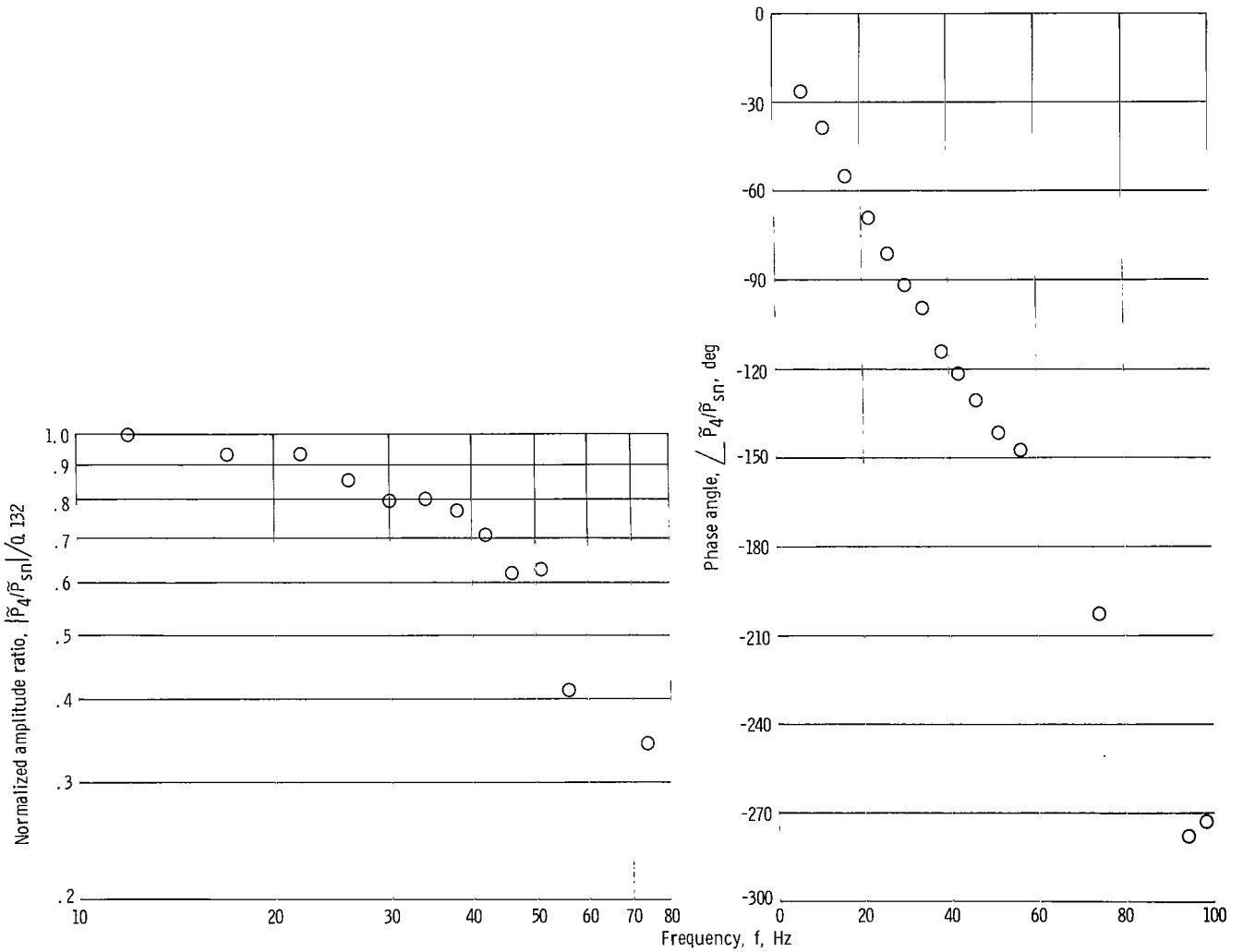

(a) Normalized amplitude ratio.

(b) Phase angle.

Figure 5. - Response of combustor pressure to spray-nozzle pressure for test A. Fuel flow, 0.052 kilogram per second; data normalized at 12 hertz.

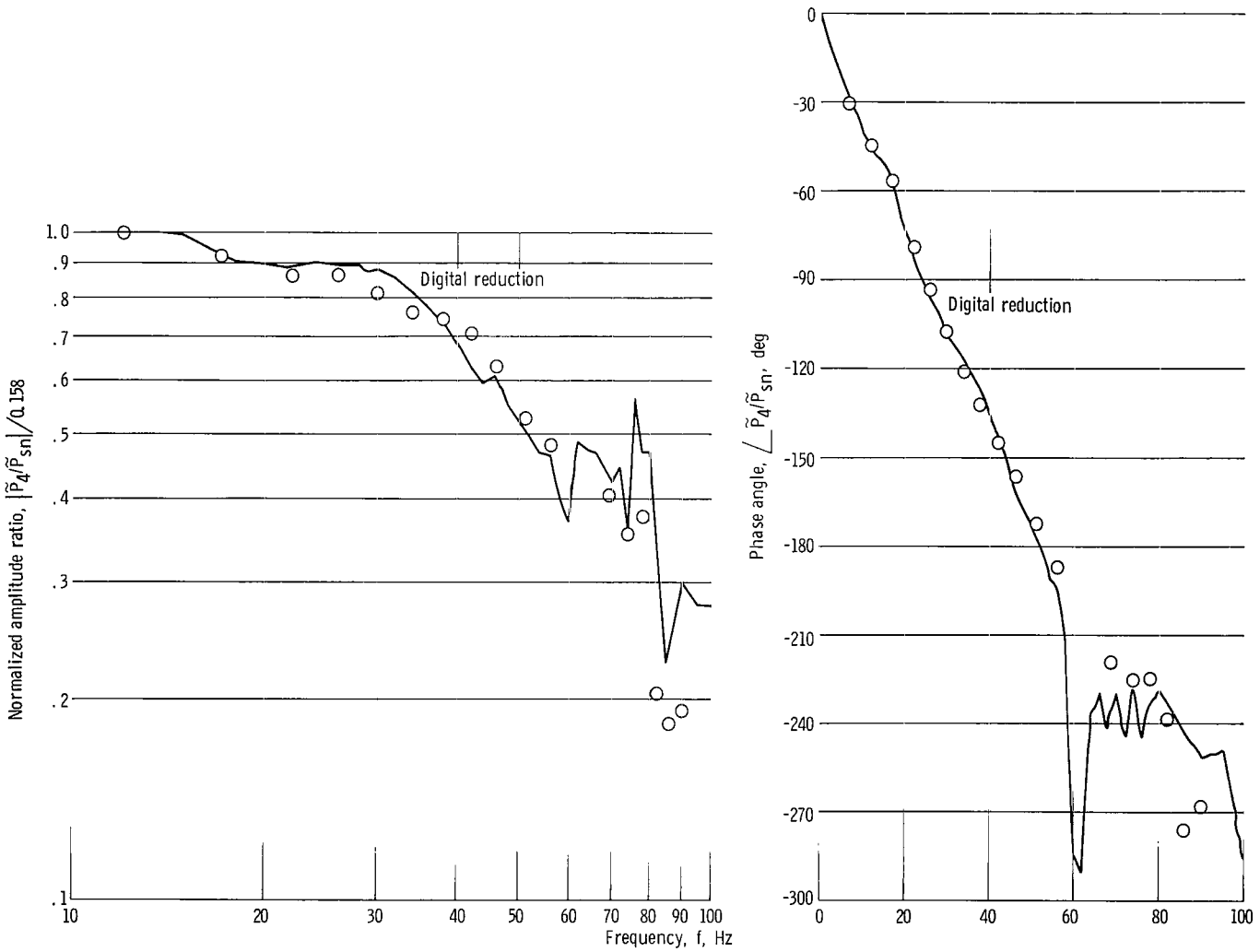

(a) Normalized amplitude ratio.

(b) Phase angle.

Figure 6. - Response of combustor pressure to spray-nozzle pressure for test B. Fuel flow, 0.076 kilogram per second; data normalized at 12 hertz.

The digitally reduced data in figure 6 show apparent resonances and antiresonances above 60 hertz. Table II indicates that the amplitudes of both the spray-nozzle-pressure and combustor-pressure oscillations are down to about 10 percent of their low-frequency values at 60 hertz. The ratio of combustor pressure to spray-nozzle pressure was formed to eliminate feed system effects. The resultant amplitude ratios are subject to the addition of errors in measuring each pressure response. Because of these low signal levels, the apparent resonances and antiresonances above 60 hertz are attributed to high noise-to-signal ratios. Phase information seemed to be less affected by the low-signal levels.

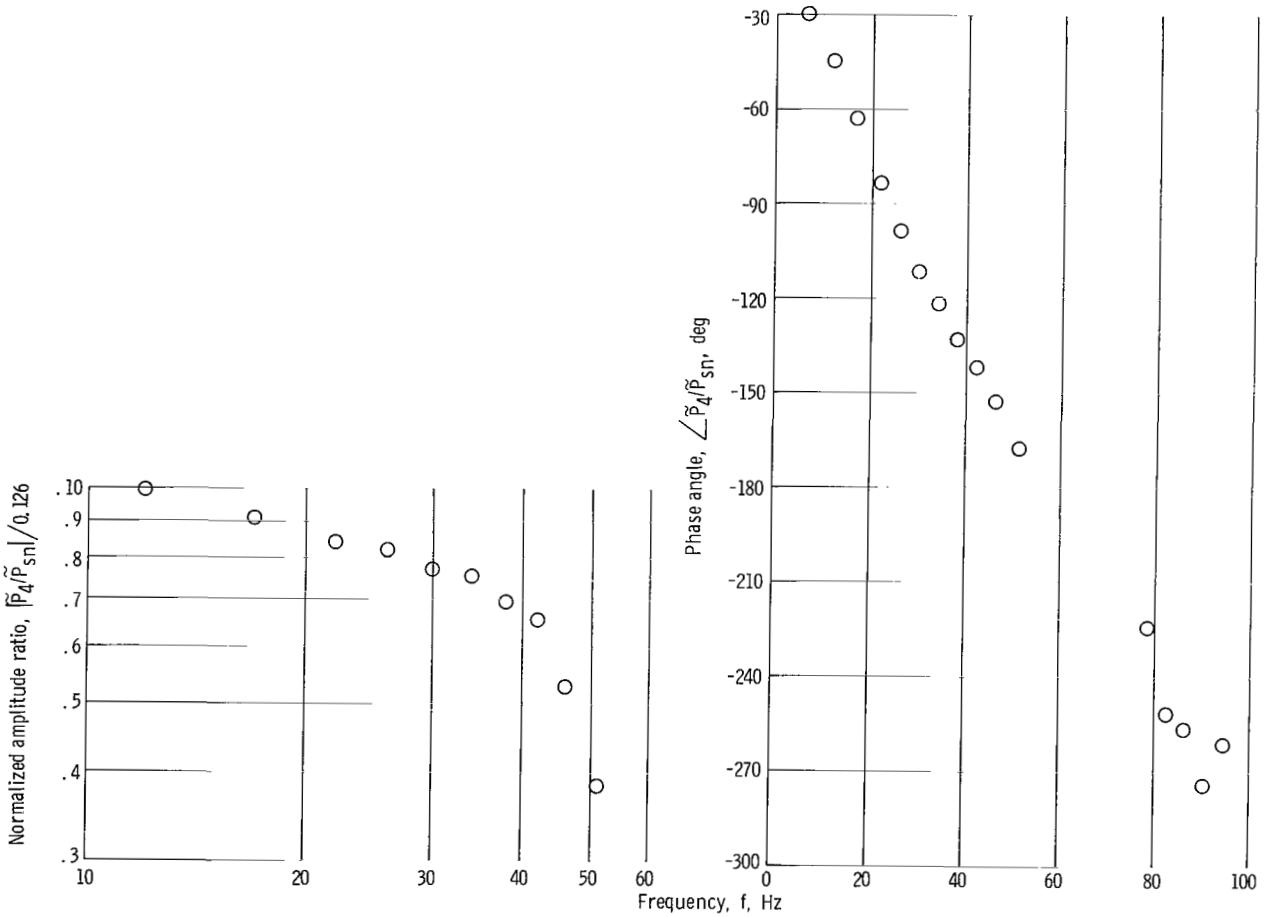

(a) Normalized amplitude ratio.

(b) Phase angle.

Figure 7. - Response of combustor pressure to spray-nozzle pressure for test C. Fuel flow, 0.092 kilogram per second; data normalized at 12 hertz.

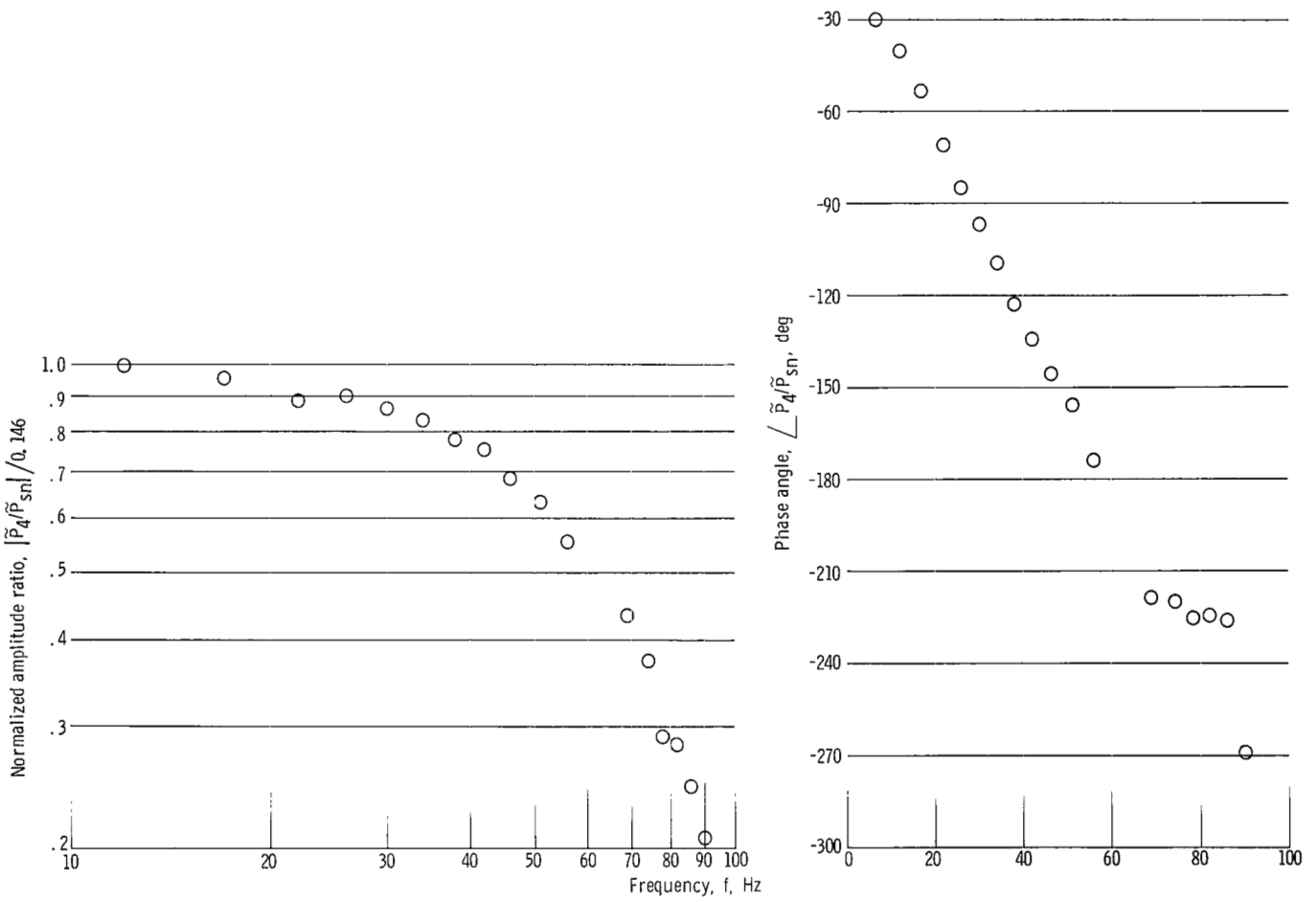

(a) Normalized amplitude ratio.

(b) Phase angle.

Figure 8. - Response of combustor pressure to spray-nozzle pressure for test D. Fuel flow, 0.106 kilogram per second; data normalized at 12 hertz.

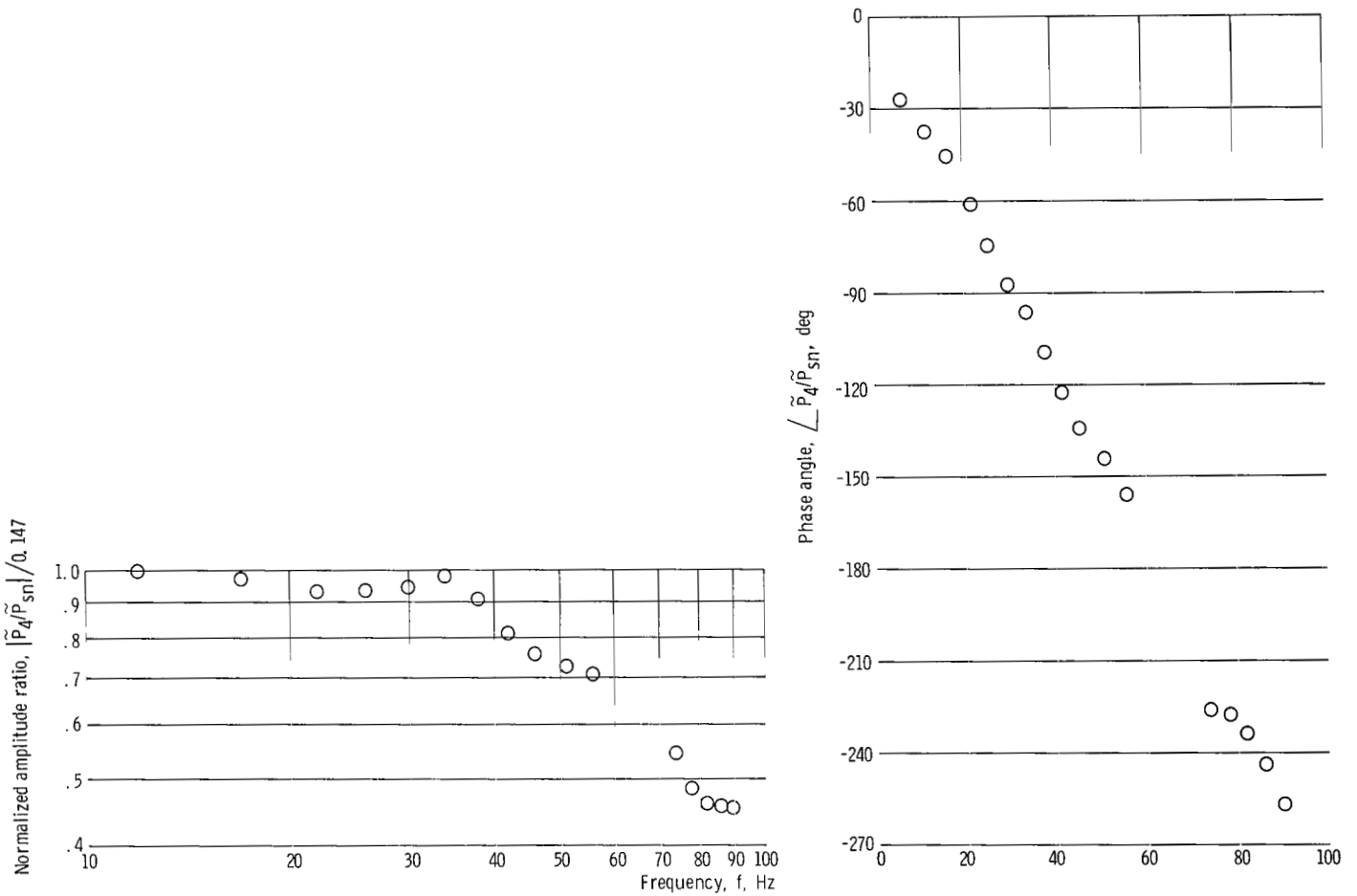

(a) Normalized amplitude ratio.

(b) Phase angle.

Figure 9. - Response of combustor pressure to spray-nozzle pressure for test E. Fuel flow, 0.132 kilogram per second; data normalized at 12 hertz.

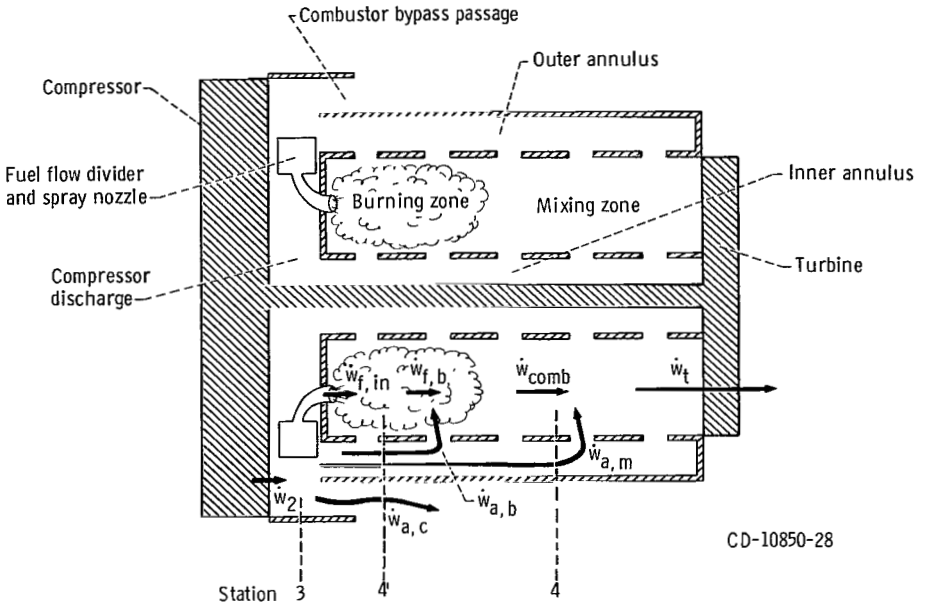

Figure 10. - Turbojet combustor model.

Analytical Model

Figure 10 is a schematic representation of the system modeled on the analog computer. The annular combustor was assumed to be made up of a primary-combustion or burning zone and a secondary-combustion or mixing zone. Pressures and thermochemical properties are computed at the midpoint of the burning and mixing zones (stations 4' and 4, respectively).

Fuel flow into the burning zone $\dot{w}_{f,\,in}$ is computed using an analog representation of the curve in figure 4. (All symbols are defined in appendix A.) The fuel is assumed to be completely vaporized and burned in the burning zone. The flow rate of burned fuel is represented by $\dot{w}_{f,\,b}$.

Thermochemical properties in the primary combustion zone for a range of fuel-to-air ratios were obtained using a digital combustion program. The resulting curves were implemented on the analog computer and are shown in figure 11. The portion of the total airflow that goes into burning $\dot{w}_{a,\,b}$ was estimated for each test using the manufacturers steady-state engine program and by assuming an energy balance through the combustor and neglecting heat transfer. By assuming that some fraction of the total airflow goes into burning, one can calculate the enthalpy in the burning zone from con-

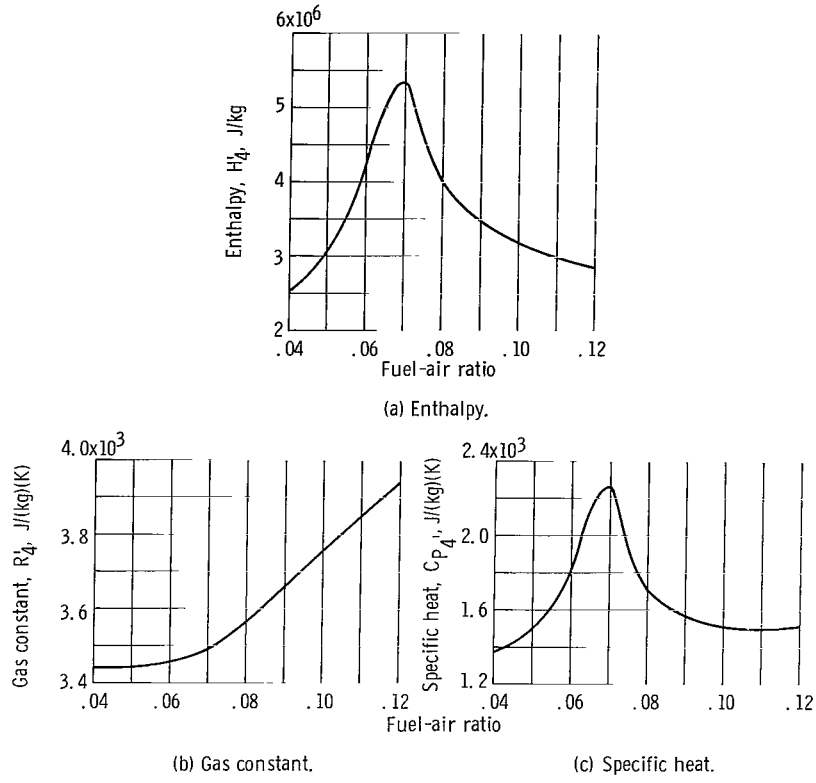

(a) Enthalpy.

(b) Gas constant.

(c) Specific heat.

Figure 11. - Thermochemical properties in burning zone as functions of fuel-to-air ratio. Fuel temperature, 322 K; air temperature 470 K; combustor pressure, 30.4 newtons per square centimeter.

ditions at the turbine entrance and compressor discharge using the standard gas mixing equation; that is,

$$\overline{H_4}\left(\overline{\dot{w}_{a,\,b}} + \overline{\dot{w}_f}\right) + \overline{H_3}\,\overline{\dot{w}_{a,\,m}} = \overline{H_4}\left(\overline{\dot{w}_{a,\,b}} + \overline{\dot{w}_{a,\,m}} + \overline{\dot{w}_f}\right) \tag{1}$$

If the calculated enthalpy H_4, agrees with that obtained from figure 11 at the assumed mixture ratio $\overline{\dot{w}_f}/\overline{\dot{w}_{a,\,b}}$, then the assumed ratio is correct. This procedure yielded the result that the fuel-to-air ratio in the burning zone is approximately 0.083 for all five tests. This value was used to estimate the steady-state airflow split. This ratio was later modified to match the observed zero-frequency amplitude ratios for the combustor-pressure to spray-nozzle-pressure responses. Analyses, described in reference 11, have pointed out that there is an effect of mixture ratio on the amplitude of the response of combustor pressure to fuel flow for rocket combustors. This result is consistent with the analytical modeling described in reference 12.

Solution of the momentum and continuity equations in the air passages, burning zone, and mixing zone (see fig. 10) required knowledge of the size of each zone. The ratio of

burning volume $V_{4'}$ to total combustor volume ($V_{4'} + V_4$) was assumed to be proportional to the square root of the steady-state ratio of burning airflow $\left(\overline{\dot{w}_{a,\,b}} + \overline{\dot{w}_{a,\,m}}\right)$. This assumption was based on results obtained for representative engines using a commercial program for annular combustors (ref. 13). This assumption agrees with the generally accepted opinion that burning takes place within about one-third of the combustor length.

The burning airflow $\dot{w}_{a,\,b}$ was assumed to travel from the compressor discharge (station 3) to the midpoint of the burning zone (station 4'). The mixing airflow $\dot{w}_{a,\,m}$ was assumed to travel from the compressor discharge to the midpoint of the mixing zone (station 4). Both burning and mixing airflows were assumed to pass through a passage having a flow area equal to the sum of the inner and outer annuli cross-sectional areas. Both flow rates were computed on the analog computer using the momentum equation with total pressure losses proportional to the square of the flow rates; that is,

$$\dot{w}_{a,\,b} = \left(\frac{g_c A}{l}\right)_b \int_0^t \left(P_3 - P_{4'} - K_b \dot{w}_{a,\,b}^2\right) d\eta + \overline{\dot{w}_{a,\,b}} \tag{2}$$

and

$$\dot{w}_{a,\,m} = \left(\frac{g_c A}{l}\right)_m \int_0^t \left(P_3 - P_4 - K_m \dot{w}_{a,\,m}^2\right) d\eta + \overline{\dot{w}_{a,\,m}} \tag{3}$$

The coefficients K_b and K_m were adjusted for each test to match the assumed airflow split and experimentally measured pressures $\overline{P}_3$ and $\overline{P}_4$.

The compressor discharge and combustor pressures were computed using the ideal gas law. At the compressor discharge, an isentropic process was assumed. This allowed, for small amplitude oscillations, the pressure to be computed from

$$P_3 = \frac{R_3 \overline{T}_3 \gamma}{V_3} \int_0^t (\dot{w}_2 - \dot{w}_{a,\,b} - \dot{w}_{a,\,m} - \dot{w}_{a,\,c}) d\eta + \overline{P}_3 \tag{4}$$

For the pressures in the burning and mixing zones, the time variation of the gas constant and temperature were included. The following equations were implemented using the curves in figure 11 and assuming that $H = C_p T$:

$$P_{4'} = \left(\frac{RH}{C_p V}\right)_{4'} \int_0^t (w_{a,\,b} + w_{f,\,b} - w_{comb}) d\eta + \overline{P}_{4'} \tag{5}$$

and

$$P_4 = \left(\frac{RH}{C_p V}\right)_4 \int_0^t (\dot{w}_{comb} + \dot{w}_{a,\,m} - \dot{w}_t)d\eta + \overline{P}_4 \tag{6}$$

Properties in the mixing zone (R_4, H_4, C_{p_4}) were determined using a form of the mixing equation (1). A time lag for the mixing process was assumed, however, with the time constant calculated using average conditions in the mixing zone; that is,

$$(\tau_m S + 1)X_4 = \beta X_3 + (1 - \beta)X_4, \tag{7}$$

$$\tau_m = \frac{\overline{V}_4 \overline{P}_4}{\overline{\dot{w}}_4} \qquad \dot{w}_4 = \dot{w}_{a,\,m} + \dot{w}_{a,\,b} + \dot{w}_{f,\,b} \tag{8}$$

$$\beta = \frac{\dot{w}_{a,\,m}}{\dot{w}_4} \tag{9}$$

where X_i is a gas property at station i.

The combustor flow $\dot{w}_{comb}$ was assumed to travel from the midpoint of the burning zone to the midpoint of the mixing zone across an area equal to the combustor annulus cross-sectional area. Only momentum pressure loss was considered (i.e., $\overline{P}_4 = \overline{P}_{4'}$) with only a very small total pressure loss included on the analog for problem stability.

The turbine and the bypass flow passage (see fig. 10) were assumed to be choked. For the turbine, the effects of the mixing-zone temperature and gas constant on flow were included. Including the momentum loss from the midpoint of the mixing zone to the turbine yielded the following expression for turbine flow:

$$\dot{w}_t = \left(\frac{g_c A}{l}\right)_t \int_0^t \left(P_4 - K_t \sqrt{\frac{R_4 H_4}{C_{P_4}}}\, \dot{w}_t\right) d\eta + \overline{\dot{w}_t} \tag{10}$$

The effects of variations in compressor discharge temperature on the bypass flow were neglected and the flow rate was assumed to be proportional to the compressor discharge pressure.

The compressor was modeled by a curve of airflow $\dot{w}_2$ versus pressure ratio P_3/P_2 for each value of corrected speed. Compressor speed, inlet pressure P_2, and inlet temperature were assumed constant for the frequency range of interest (above 7 Hz).

Data for the compressor curves were obtained from the steady-state engine program using the same compressor-face conditions (pressure, temperature, Mach number).

Table I(b) contains a summary of the steady-state operating conditions used in the analog simulation. Total airflow to the combustor was assumed to be equal to that given by the steady-state engine program. The listed burning and mixing airflows correspond to the burning-zone mixture ratios that gave the proper zero-frequency amplitude ratio for the combustor to spray-nozzle pressure response. Because of the high temperatures and potential turbine damage, no temperature measurements were made in the combustor. The listed values for enthalpy are based on the steady-state engine program and adjusted burning-zone mixture ratio.

To allow flexibility in fitting the frequency response data, the following form was assumed for the fuel combustion dynamics:

$$\dot{w}_{f,\,b} = \frac{\dot{w}_{f,\,in} e^{-\sigma s}}{(aS^2 + bS + 1)} \tag{11}$$

where a and b are related to the familiar natural frequency and damping ratio for a second-order system by

$$a = \frac{1}{\omega_c^2}$$

$$b = \frac{2\xi_c}{\omega_c}$$

The parameters σ, a, and b were adjusted on the analog for each operating condition to best match the experimental responses shown in figures 5 to 9.

The mixing time constant τ_m could also be adjusted on the analog computer, but its effect was slight and good agreement was obtained using the calculated values for each operating condition. Appendix B contains a summary of the integral equations implemented on the analog computer.

Sinusoidal oscillations in spray-nozzle pressure were simulated on the analog computer using a transfer-function analyzer and its associated oscillator. The analyzer was used to determine the amplitude ratio and relative phase angle for the response of the mixing-zone pressure P_4 to oscillations in the spray-nozzle pressure P_{sn}. The mixing-zone pressure, rather than the burning-zone pressure $P_{4'}$, was selected because the experimental transducer was located in the mixing zone (see fig. 2).

Comparison of experimental and computer responses. - Figures 12 to 16 show comparisons between the experimental and simulation responses of combustor pressure P_4 to spray-nozzle pressure P_{sn}. Table II contains the simulation data from which the plots were generated.

In all cases, the response could be matched closely using the mixing-zone lag, as described in equations (7) to (9), and the form of fuel combustion dynamics given by equation (11). The shape of the frequency response plot was matched as well as possible by manipulating only the parameters a and b (see eq. (11)). The parameter a had the greater effect at the higher frequencies, and the parameter b was used to adjust the amplitude response near the natural frequency $1/2\pi \sqrt{a}$. Because of the closed-loop nature of the response (combustor pressure affects fuel flow through the spray nozzles), the dead time σ had a slight effect on the amplitude ratio. However, the dead time was adjusted to best match the phase angle at high frequencies for the selected values of a and b. Once approximate values of a, b, and σ were obtained, adjustments were made to best fit the amplitude and phase responses. For all cases, the required fuel combustion natural frequency $1/2\pi \sqrt{1/a}$ was 55 hertz. The damping ratio $b/2\sqrt{a}$ had to be reduced from 0.70 to 0.55 and 0.50 at the higher flow rates (tests D and E, respectively). The slower fall-off in amplitude ratio at the higher fuel flows was attributed to the burning zone expanding downstream (ref. 5). The need to decrease the combustion process damping arose from the fact that the analog simulation assumed a fixed distance (one-half the combustor length) between the primary combustion and pressure measurement locations.

As mentioned previously, the amplitude ratio at very low frequencies was matched by adjusting the burning-zone mixture ratio on the computer. While maintaining constant fuel and total airflows to the combustor, the split of airflow between the burning and mixing zones was adjusted by changing the pressure drop coefficients K_b and K_m (eqs. (2) to (3)). Figure 17 shows the resulting effect of the burning-zone mixture ratio on the zero-frequency amplitude ratio for test B. The experimentally observed zero-frequency amplitude ratio of 0.158 corresponds to a burning-zone fuel-to-air ratio of 0.0906. This procedure was repeated for each of the selected tests prior to the matching of the frequency-response data. Table III summarizes the simulation combustion parameters a, b, and σ and the burning-zone mixture ratios that gave a satisfactory match of simulation and experimental frequency-response data. Figure 18 is a plot of the ratio of burning-zone volume to total combustor volume as a function of fuel flow. The volume ratio is based on the assumed airflow distribution (ref. 13) with the adjusted burning-zone mixture ratios. The dashed-curve is a fit of the data points, passing through the origin. Figure 18 shows the expansion of the burning-zone downstream for increased fuel flow to maintain mixture ratio in the range of 0.083 to 0.093. The higher mixture

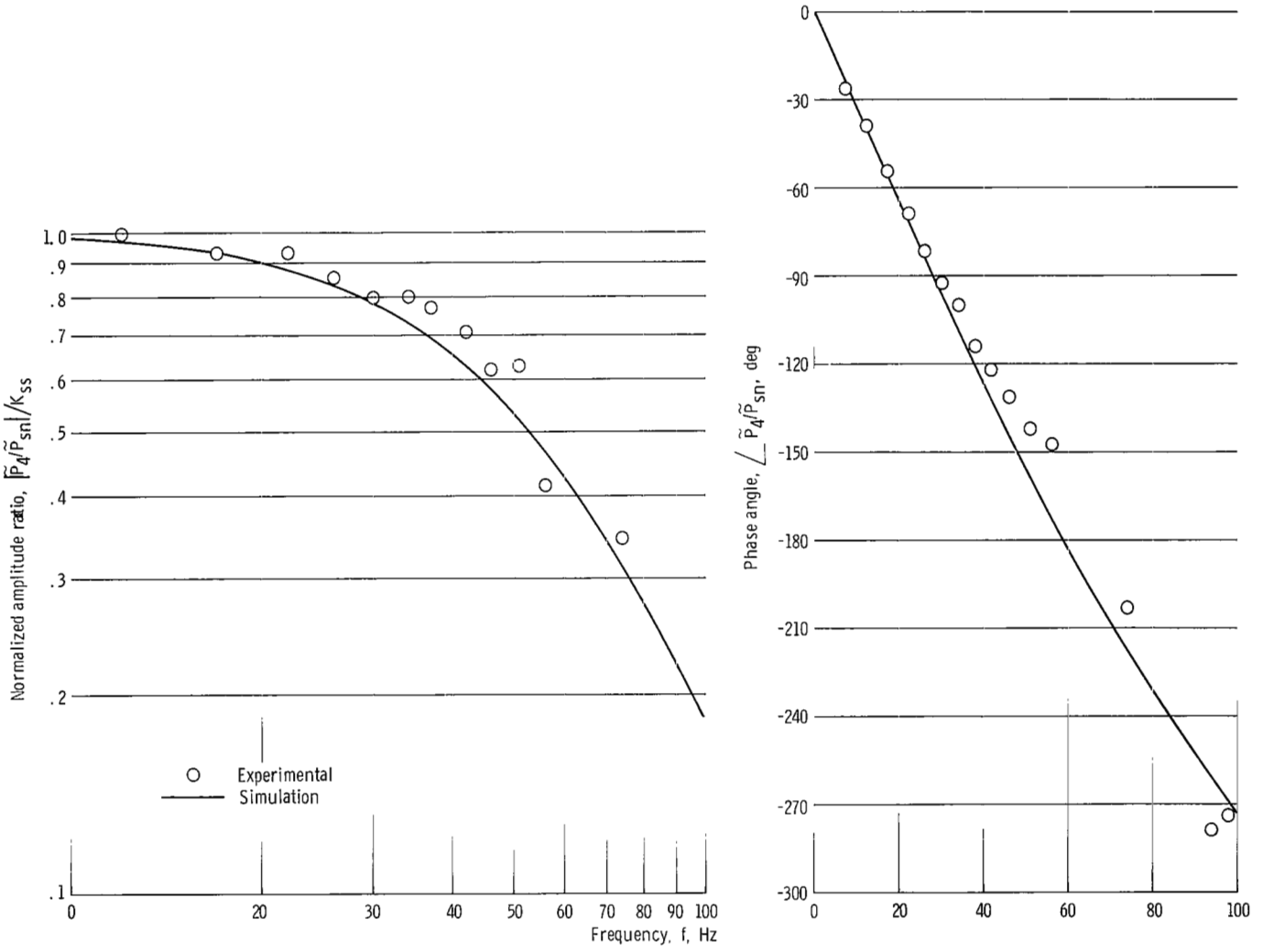

(a) Normalized amplitude ratio.

(b) Phase angle.

Figure 12. - Comparison of experimental and simulation responses of combustor pressure to spray-nozzle pressure for test A. Fuel flow, 0.052 kilogram per second; zero-frequency amplitude, 0.132; a fuel-to-air ratio, 0.0832; dead time, 2.60 milliseconds; mixing-zone time constant, 1.84 milliseconds; natural frequency, 55 hertz; damping ratio for fuel combustion dynamics, 0.70.

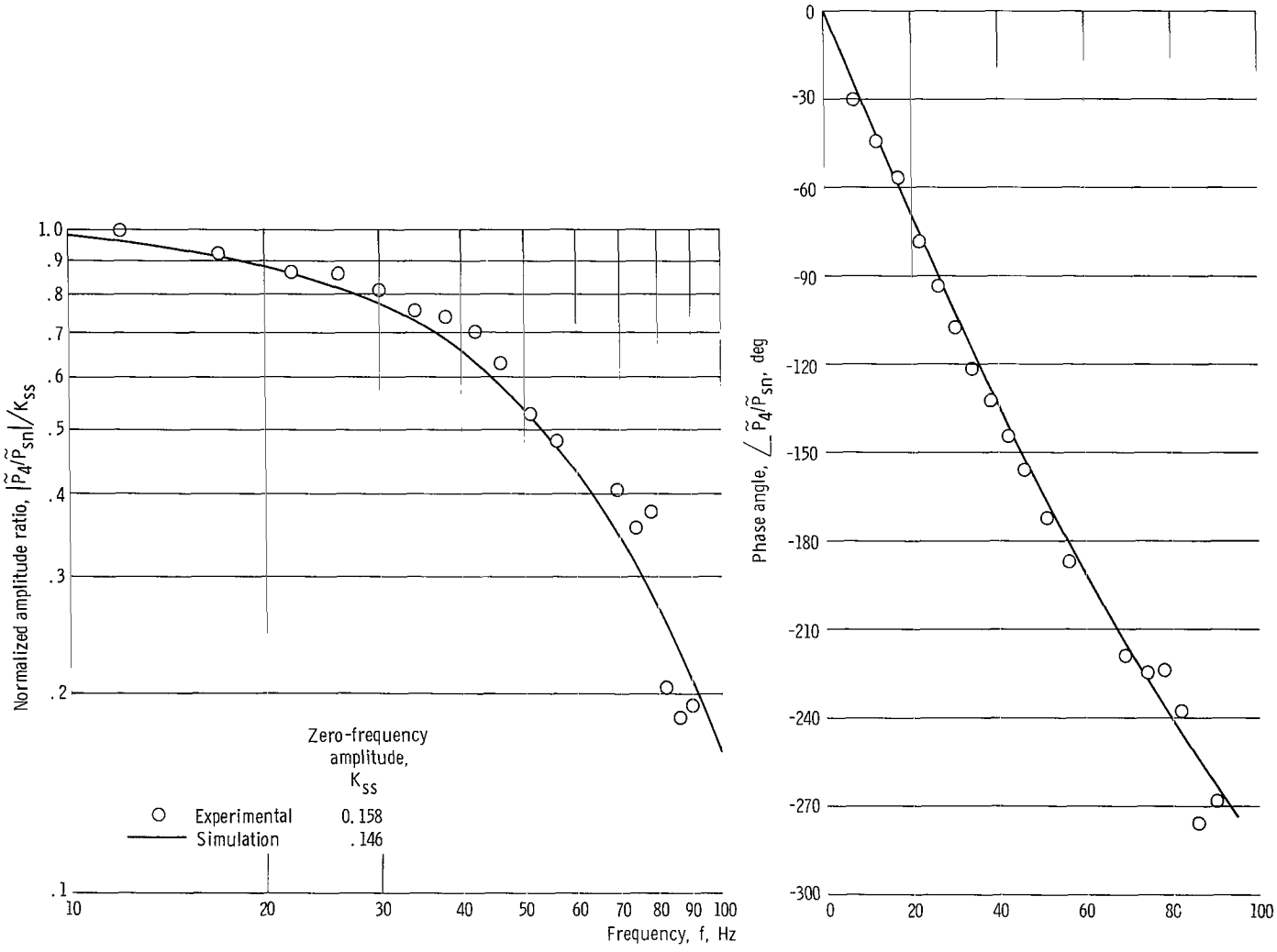

(a) Normalized amplitude ratio.

(b) Phase angle.

Figure 13. - Comparison of experimental and simulation responses of combustor pressure to spray-nozzle pressure for test B. Fuel flow, 0.76 kilogram per second; fuel-to-air ratio, 0.0918; dead time, 3.00 milliseconds; mixing-zone time constant, 1.83 milliseconds; natural frequency, 55.0 hertz; damping ratio for fuel combustion dynamics, 0.70.

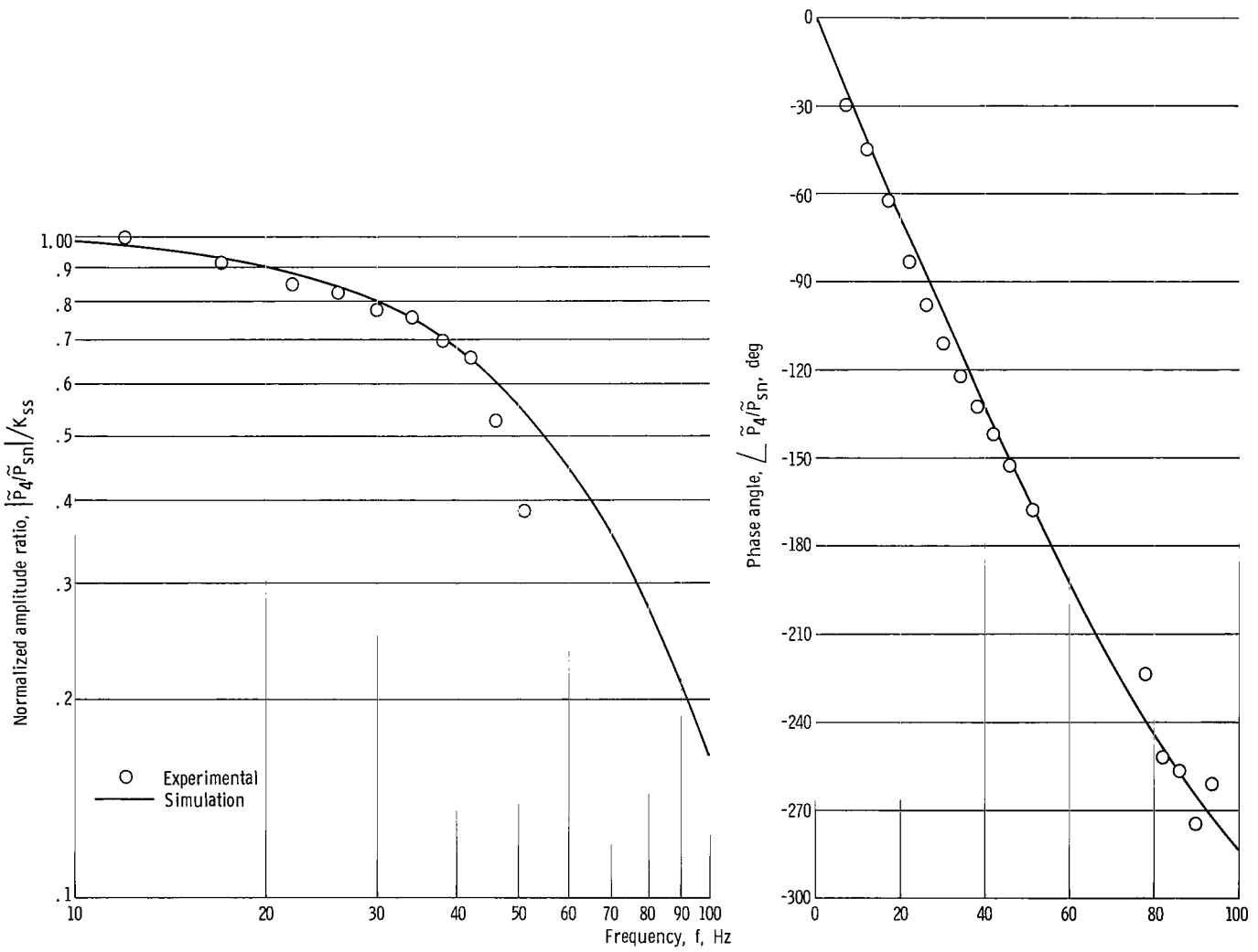

(a) Normalized amplitude ratio.

(b) Phase angle.

Figure 14. - Comparison of experimental and simulation responses of combustor pressure to spray-nozzle pressure for test C. Fuel flow, 0.092 kilogram per second; zero-frequency amplitude, 0.126; fuel-to-air ratio, 0.0932; dead time, 3.20 milliseconds; mixing-zone time constant, 1.67 milliseconds; natural frequency, 55 hertz; damping ratio for fuel combustion dynamics, 0.70.

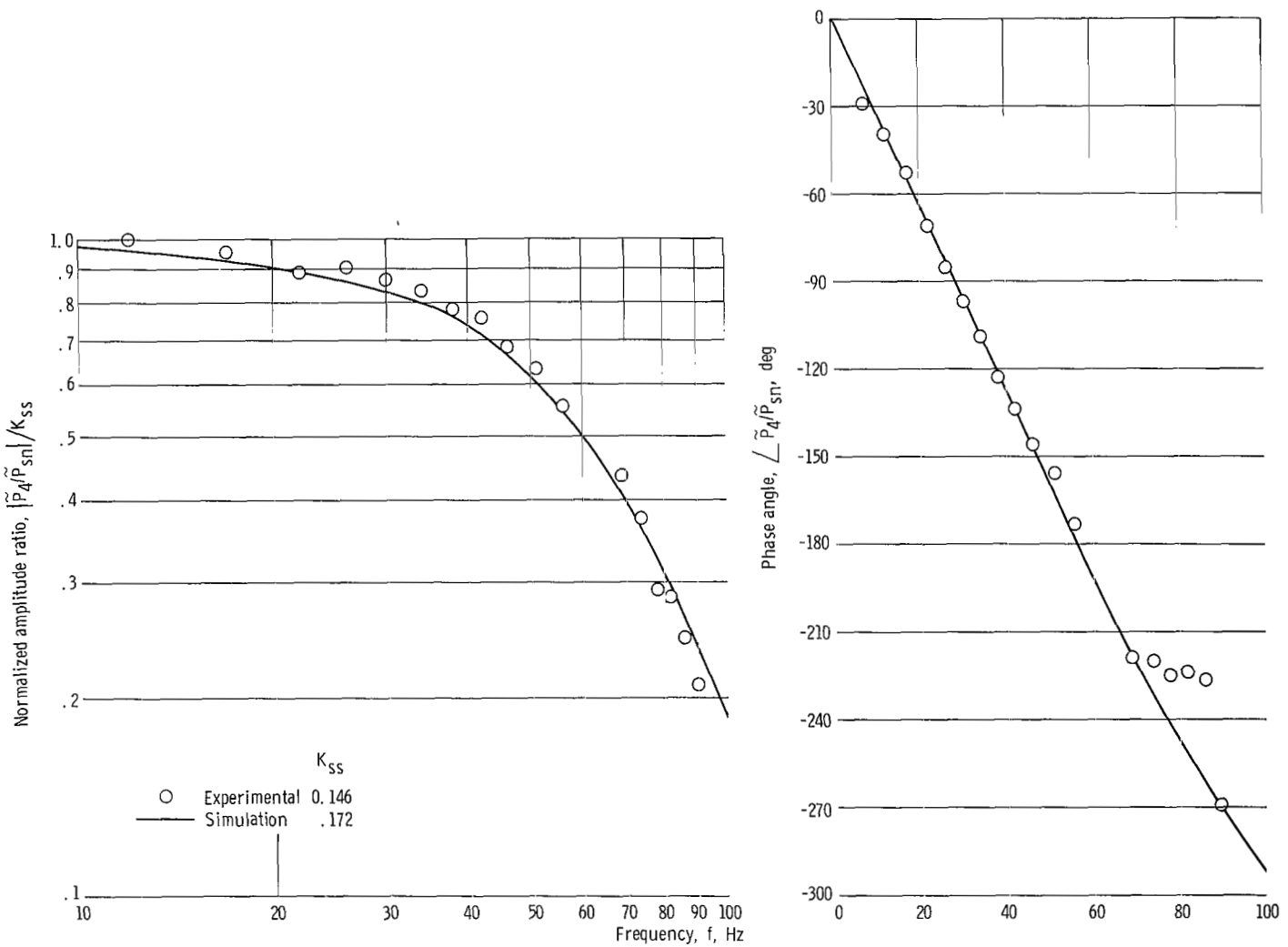

(a) Normalized amplitude ratio.

(b) Phase angle.

Figure 15. - Comparison of experimental and simulation responses of combustor pressure to spray-nozzle pressure for test D; fuel flow, 0.106 kilogram per second; fuel-to-air ratio, 0.0863; dead time, 3.00 milliseconds; mixing-zone time constant, 1.37 milliseconds; natural frequency, 55 hertz; damping ratio for fuel combustion dynamics, 0.55.

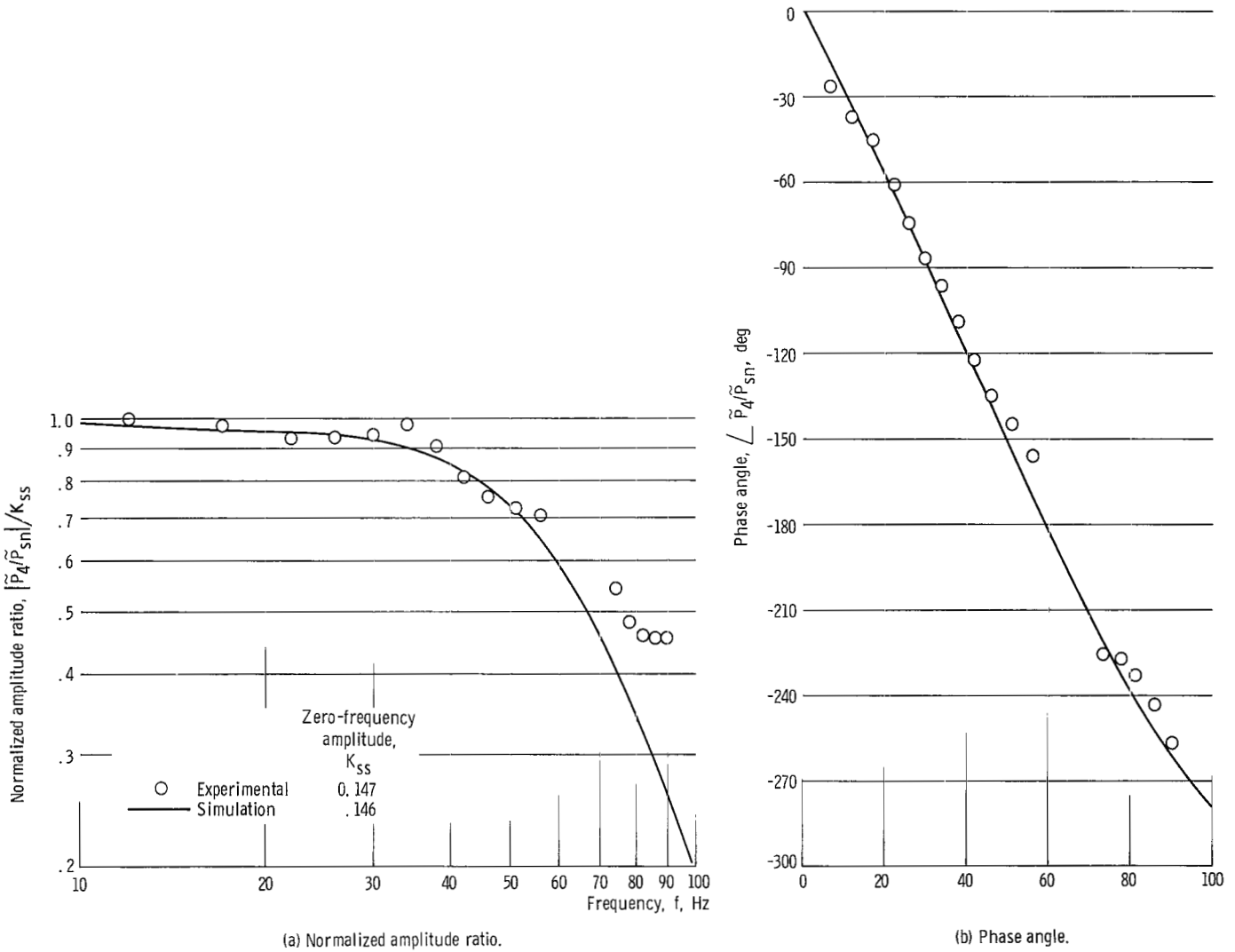

(a) Normalized amplitude ratio.

(b) Phase angle.

Figure 16. - Comparison of experimental and simulation responses of combustor pressure to spray-nozzle pressure for test E. Fuel flow, 0.132 kilogram per second; fuel-to-air ratio, 0.0874; dead time, 2.60 milliseconds; mixing-zone time constant, 1.33 milliseconds; natural frequency, 55 hertz; damping ratio for fuel combustion dynamics, 0.50.

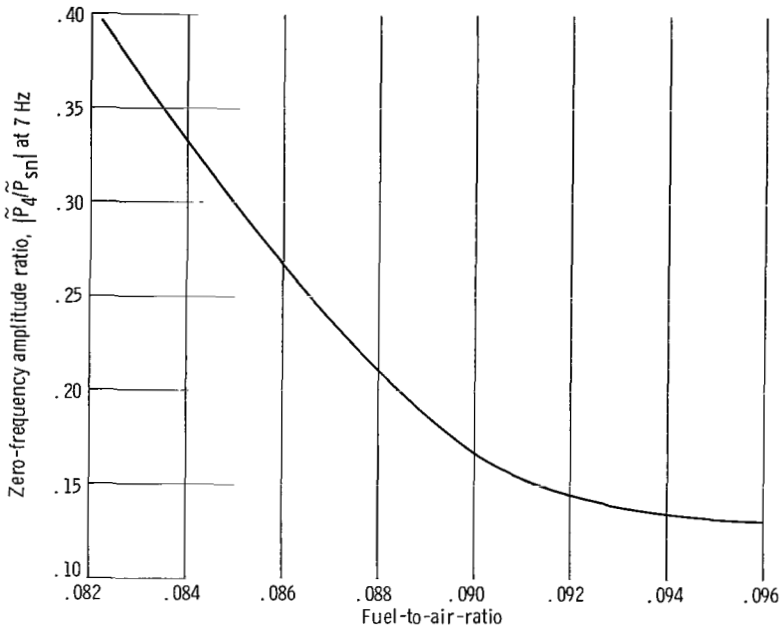

Figure 17. - Sensitivity of zero-frequency amplitude ratio to fuel to air ratio in burning zone for test B. Fuel flow, 0.076 kilogram per second; total combustor air flow, 11.3 kilograms per second (simulation data).

TABLE III. - COMBUSTION AND MIXING DYNAMICS REQUIRED FOR MATCHING OF SIMULATION AND EXPERIMENTAL FREQUENCY RESPONSES OF COMBUSTION PRESSURE SPRAY NOZZLE PRESSURE

[Natural frequency corresponding to coefficient a, 55.0 Hz.]

Test	Fuel-to-air ratio in burning zone	Steady-state amplitude ratio		Calculated mixing-zone time constant, τ_m, sec	Selected dead time for best match of responses, σ, sec	Selected coefficient for best match of responses		Damping ratio corresponding to coefficient b
		Experimental	Simulation			a, sec^2	b, sec	
A	0.0832	0.132	0.132	1.84×10^{-3}	2.60×10^{-3}	8.37×10^{-6}	4.05×10^{-3}	0.70
B	.0918	.158	.146	1.83	3.00	8.37	4.05	.70
C	.0932	.126	.126	1.67	3.20	8.37	4.05	.70
D	.0863	.146	.172	1.37	3.00	8.37	3.18	.55
E	.0874	.147	.146	1.33	2.60	8.37	2.89	.50

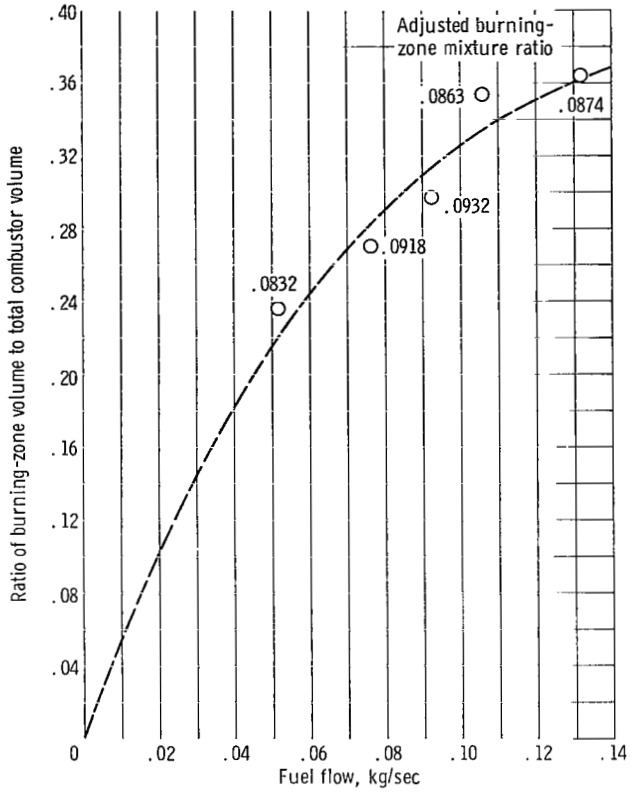

Figure 18. - Effect of fuel flow on burning-zone volume (based on match of zero-frequency amplitude ratio).

ratios result in lower zero-frequency amplitude ratios because of the slopes of the thermochemical curves (fig. 11).

Curve-fit of experimental data. - It was demonstrated that the analog simulation could adequately match the experimental frequency responses. The responses obtained from the simulation, however, were dominated by the dead time and second-order lag (natural frequency of 55 Hz) used for the fuel-combustion dynamics. These values were assumed rather than calculated. Thus, the contribution of the simulation was to provide the first-order mixing dynamics and higher frequency effects due to the combustor geometry, etc. It also closed the feedback loop whereby fuel flow $\dot{w}_{f,\,in}$ was decreased as the combustor pressure P_4, increased. In the case of the J85 combustor operating at the selected test conditions, the effect of the feedback is slight. Thus, the closed-loop response characteristics (i.e., natural frequency and damping) were changed only slightly relative to their open-loop values. Therefore, we concluded that the useful transfer functions could be obtained more directly by curve-fitting the experimental data. The zero-frequency amplitude ratio could then be obtained from the burning-zone fuel-to-air ratio determination.

Accordingly, a dead-time, first-order-lag second-order-lag combination was selected to match the closed-loop frequency responses; that is,

$$\frac{\tilde{P}_4}{\tilde{P}_{sn}} = \frac{K_{ss}e^{-C_1S}}{(C_2S + 1)\left(C_3S^2 + C_4S + 1\right)} \tag{13}$$

Different symbols were selected for this transfer function to distinguish it from the open-loop transfer function used in the simulation.

Figure 19 shows a comparison of experimental and curve-fit responses for test B. Using the same procedure as outlined in the previous section, the transfer-function parameters were ajdusted to best fit the experimental data. For simplicity, the first-order time constant C_2 was set equal to the calculated mixing time constant (eq. (8)): Table IV summarizes the results of the curve-fitting for all tests. The second-order natural frequency $1/2\pi\sqrt{1/C_3}$ was 55 hertz for all tests. This result indicated that the combustion dynamics, as determined on the analog computer, dominate the closed-loop response of combustor pressure to spray-nozzle pressure. As was the case with the simulation damping ratio $b/2\sqrt{a}$, the curve-fit damping ratio $C_4/2\sqrt{C_3}$ had to be decreased at the higher fuel flows. For all tests, the magnitude of $C_4/2\sqrt{C_3}$ was greater than $b/2\sqrt{a}$. Except for test E, which had the highest fuel flow rate, the curve-fit dead time C_1 was equal to the simulation value σ. For test E, the curve-fit value was slightly higher (3.0 msec compared with 2.6 msec).

For frequencies below about 50 hertz, the response of the J85 combustor pressure to fuel spray-nozzle pressure could be approximated by the dead time C_1 and a first-order lag having a time constant equal to the sum of C_2 and C_4 (see table IV). It should

TABLE IV. - CURVE-FIT PARAMETERS FOR BEST FIT OF COMBUSTOR PRESSURE TO SPRAY-NOZZLE PRESSURE EXPERIMENT RESPONSE

Test	Steady-state amplitude ratio	Dead time, C_1, sec	First-order time constant,[a] C_2, sec	Second-order lag coefficients		Sum of coefficients C_2 and C_4, sec	Natural frequency corresponding to C_3, Hz	Damping ratio corresponding to C_4
				C_3, sec^2	C_4, sec			
A	0.132	2.6×10^{-3}	1.84×10^{-3}	8.37×10^{-6}	4.97×10^{-3}	6.76×10^{-3}	55.0	0.85
B	.158	3.0	1.83	8.37	5.21	7.04	55.0	.90
C	.126	3.2	1.67	8.37	5.21	6.88	55.0	.90
D	.146	3.0	1.37	8.37	4.74	6.11	55.0	.82
E	.147	3.0	1.33	8.37	4.05	5.38	55.0	.70

[a]Assumed equal to mixing time constant.

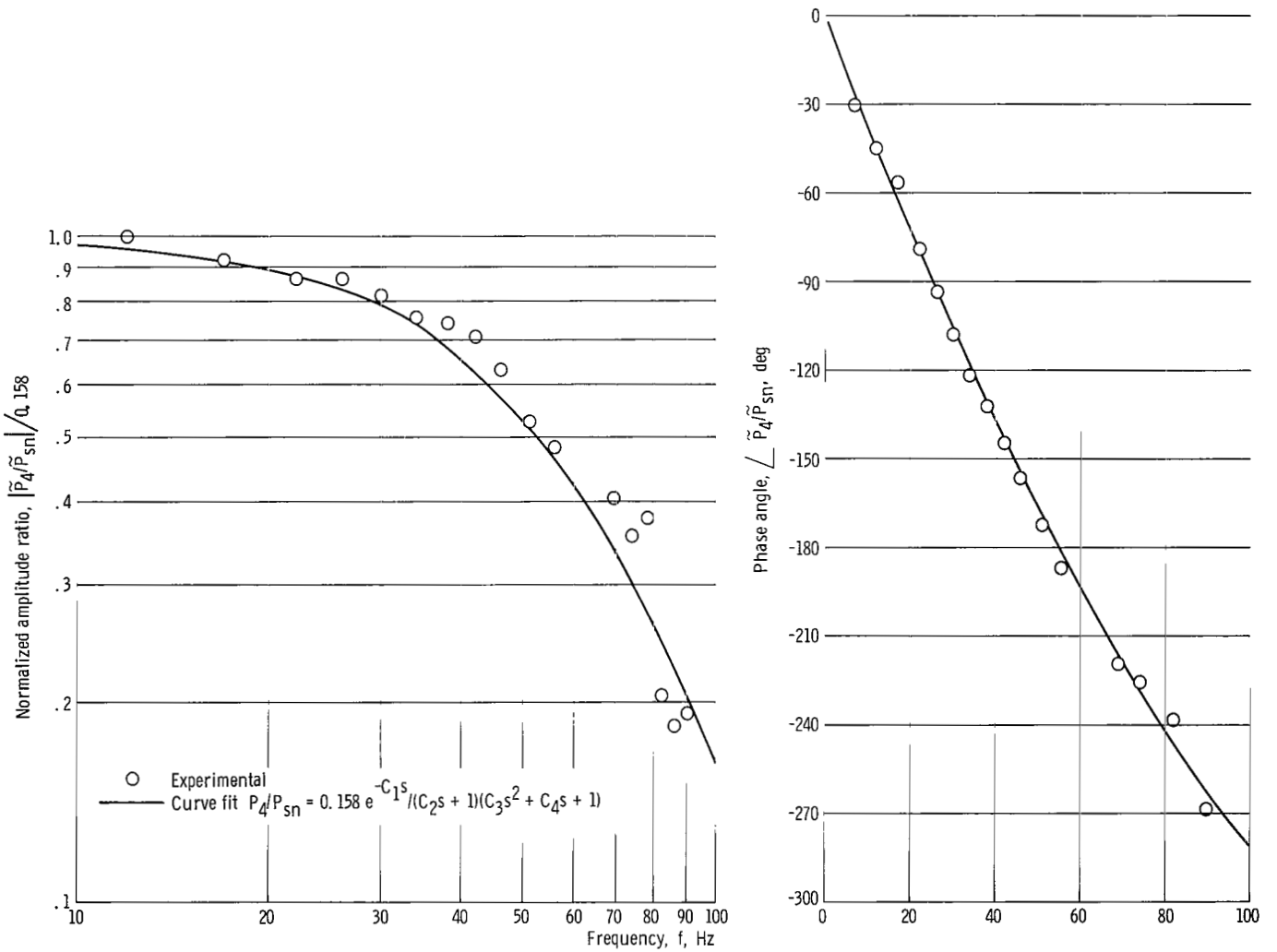

(a) Normalized amplitude ratio.

(b) Phase Angle.

Figure 19. - Comparison of experimental and curve-fit responses of combustor pressure to spray-nozzle pressue for test B. Fuel flow, 0.076 kilogram per second. Curve fit values: dead time, 3.00 milliseconds; first-order coefficient C_2, 1.83 milliseconds; second-order coefficient C_3, 8.37×10^{-6} second squared; second-order coefficient C_4, 5.21 milliseconds. Natural frequency, 55 hertz; damping ratio for curve-fit frequency response, 0.9.

be noted that the sum of C_2 and C_4 is close to the 8-millisecond lag observed for lower frequencies in reference 5. Below about 30 hertz, the response could be approximated by the constant zero-frequency amplitude ratio K_{ss}.

SUMMARY OF RESULTS

Experimental data obtained from sweep-frequency testing of a J85 turbojet engine were analyzed to determine the response of combustor pressure to fuel spray-nozzle pressure oscillations. Frequency response characteristics were displayed for all tests in the form of Bode plots.

To match the experimental data and to identify the source of the observed dynamics, an analytical model was developed and implemented on the analog computer. The following results were obtained from the simulation:

1. A dead-time - second-order-lag form for the fuel combustion dynamics was required to match the experimental data.

2. Dead time was relatively insensitive to fuel flow. It varied from 2.6 to 3.2 milliseconds over the range of flows encountered.

3. The second-order-combustion lag had a natural frequency of 55 hertz which was not affected by the operating conditions. The damping ratio had to be decreased for increasing fuel flow, varying from 0.70 to 0.50. This effect was attributed to an expansion of the burning zone downstream toward the combustor pressure transducer.

4. For fixed flows to the combustor, the zero-frequency amplitude ratio for the combustor pressure to spray-nozzle pressure response was a strong function of the burning zone fuel-to-air ratio. Burning-zone mixture ratios were computed for each test condition. This information, together with an assumed airflow distribution into the combustor, indicated that the burning zone does expand to maintain the fuel-to-air ratio relatively constant (0.083 to 0.093 over the range of fuel flows considered).

Transfer functions, obtained from curve-fitting the experimental data, were also determined. The following results were obtained from the curve-fitting:

1. The response of combustor pressure to spray-nozzle pressure could be fit by a dead-time - first-order-lag - second-order-lag combination.

2. The curve fit dead time matched the simulation value for all tests except the higher fuel flow case.

3. The first-order-lag term was related to the mixing process in the combustor, and the time constant was calculated from steady-state conditions in the combustor and varied from 1.33 to 1.84 milliseconds.

4. The second-order natural frequency was equal to the simulation fuel combustion natural frequency. The curve-fit damping ratio had to be decreased at the higher fuel

flows but exceeded the simulation combustion value for all tests. It varied from 0.90 to 0.70.

5. Below about 50 hertz, the response could be fit by a dead time and a first-order lag.

6. Below about 30 hertz, the response was relatively flat (+0, -2.3 db).

Lewis Research Center,
National Aeronautics and Space Administration,
Cleveland, Ohio, July 22, 1970,
720-03.

APPENDIX A

SYMBOLS

A	cross-sectional area, m^2
a	coefficient in simulation fuel-combustion dynamics, sec^2
b	coefficient in simulation fuel-combustion dynamics, sec
C_p	specific heat of combustion products, J/(kg)(K)
C_1	curve-fit dead time, sec
C_2	curve-fit first-order time constant, sec
C_3	curve-fit second-order coefficient, sec^2
C_4	curve-fit second-order coefficient, sec
f_j	functional relation where j = 1, 2, 3, 4, 5
g	gravitational acceleration, m/sec^2
g_c	gravitational constant, $1(kg)(m)/(N)(sec^2)$
H	total enthalpy, J/kg
K	pressure-drop coefficient, $(N)(sec^2)/(m^2)(kg^2)$
K_c	choked restriction coefficient, $(kg)(m^2)/(N)(sec)$
K_{ss}	zero-frequency amplitude ratio
K_t	turbine coefficient, $(N^{1/2})(sec)/(kg^{1/2})(m^{5/2})$
l	length, m
N	compressor speed, rpm
P	total pressure, N/m^2
R	gas constant, J/(kg)(K)
S	Laplace operator, sec^{-1}
T	total temperature, K
t	time, sec
V	volume, m^3
$\dot{w}$	mass flow rate, kg/sec
X_i	fluid property at station i, i = 2, 3, 4, 4'
β	ratio of mixing airflow to total combustor airflow
γ	specific heat ratio
η	variable of integration, sec
ξ_c	damping ratio for fuel combustion dynamics
ξ_s	damping ratio for curve fit of frequency response
σ	dead time in simulation combustion dynamics, sec
τ	time constant, sec
ω_c	natural frequency for fuel-combustion dynamics, rad/sec
ω_s	natural frequency for curve fit of frequency response, rad/sec

Subscripts:

a	air
b	burning path from station 4' to 4

c	cooling path from station 3 to 4
comb	combustor path from station 4' to 4
f	fuel
in	injected
m	mixing zone
sn	spray nozzle
t	turbine

Superscripts:

—	steady-state value of variable
~	sinusoidally varying component of variable

APPENDIX B

SIMULATION EQUATIONS

$$P_2 = \text{Constant} = \overline{P}_2 \tag{B1}$$

$$N = \text{Constant} = \overline{N} \tag{B2}$$

$$\dot{w}_{a,\,b} = \left(\frac{g_c A}{l}\right)_b \int_0^t \left(P_3 - P_{4'} - K_b \dot{w}_{a,\,b}^2\right) d\eta + \overline{\dot{w}}_{a,\,b} \tag{2}$$

$$\dot{w}_{a,\,m} = \left(\frac{g_c A}{l}\right)_m \int_0^t \left(P_3 - P_4 - K_m \dot{w}_{a,\,m}^2\right) d\eta + \overline{\dot{w}}_{a,\,m} \tag{3}$$

$$P_3 = \frac{R_3 \overline{T}_3 \gamma_3}{V_3} \int_0^t (\dot{w}_2 - \dot{w}_{a,\,b} - \dot{w}_{a,\,m} - \dot{w}_{a,\,c}) d\eta + \overline{P}_3 \tag{4}$$

$$\dot{w}_2 = f_1\left(\frac{P_3}{P_2},\ N\right) \tag{B3}$$

$$\dot{w}_{a,\,c} = K_c P_3 \tag{B4}$$

$$\dot{w}_{f,\,in} = f_2(P_{sn} - P_4) \tag{B5}$$

$$P_{4'} = \left(\frac{RH}{C_p V}\right)_{4'} \int_0^t (\dot{w}_{a,\,b} + \dot{w}_{f,\,b} - \dot{w}_{comb}) d\eta + \overline{P}_{4'} \tag{5}$$

$$\ddot{w}_{f,\,b} = \frac{1}{a} \int_0^t \left[\dot{w}_{f,\,in}(t - \sigma) - \dot{w}_{f,\,b} - b\ddot{w}_{f,\,b}\right] d\eta \tag{B6}$$

$$\dot{w}_{f,\,b} = \int_0^t \ddot{w}_{f,\,b}\, d\eta + \overline{\dot{w}}_f \tag{B7}$$

$$R_{4'} = f_3 \frac{\dot{w}_{f,b}}{\dot{w}_{a,b}} \tag{B8}$$

$$H_{4'} = f_4 \frac{\dot{w}_{f,b}}{\dot{w}_{a,b}} \tag{B9}$$

$$C_{p,4'} = f_5 \frac{\dot{w}_{f,b}}{\dot{w}_{a,b}} \tag{B10}$$

$$V_{4'} = \sqrt{\frac{\overline{\dot{w}_{a,b}}}{(\dot{w}_{a,b} + \dot{w}_{a,c})(V_{4'} + V_4)}} \tag{B11}$$

$$\dot{w}_{comb} = \left(\frac{g_c A}{l}\right)_{comb} \int_0^t (P_{4'} - P_4)d\eta + \overline{\dot{w}_{comb}} \tag{B12}$$

$$P_4 = \left(\frac{RH}{C_p V}\right)_4 \int_0^t (\dot{w}_{comb} + \dot{w}_{a,m} - \dot{w}_t)d\eta + P_4 \tag{6}$$

$$R_4 = \frac{1}{\tau_m} \int_0^t \left[\beta R_3 + (1 - \beta)R_{4'} - R_4\right]d\eta + \overline{R_4} \tag{B13}$$

$$H_4 = \frac{1}{\tau_m} \int_0^t \left[\beta H_3 + (1 - \beta)H_{4'} - H_4\right]d\eta + \overline{H_4} \tag{B14}$$

$$C_{p_4} = \frac{1}{\tau_m} \int_0^t \left[\beta C_{p_3} + (1 - \beta)C_{p_{4'}} - C_{p_4}\right]d\eta + \overline{C_{p_4}} \tag{B15}$$

$$\beta = \frac{\dot{w}_{a,m}}{(\dot{w}_{a,m} + \dot{w}_{a,b} + \overline{\dot{w}_{f,b}})} \tag{B16}$$

$$\dot{w}_t = \left(\frac{g_c A}{l}\right)_t \int_0^t \left(P_4 - K_t \sqrt{\frac{R_4 H_4}{C_{p_4}}}\, \dot{w}_t\right) d\eta + \overline{\dot{w}_t} \qquad (10)$$

REFERENCES

1. Craig, R. T.; Nakanishi, S.; and Wile, D. B.: Analytical and Experimental Study of Transient-Response Characteristics of a Turboprop Engine. NACA RM E55C23, 1955.

2. McCafferty, Richard J.; and Donlon, Richard H.: Transient and Steady-State Performance of a Single Turbojet Combustor with Four Different Fuel Nozzles. NACA RM E55H03a, 1955.

3. Gold, Harold; and Straight, David M: Gas-Turbine-Engine Operation with Variable-Area Fuel Nozzles. NACA RM E8D14, 1948.

4. Conrad, E. William; Bloomer, Harry E.; and Sobolewski, Adam E.: Altitude Operational Characteristics of a Prototype Model of the J47D (RX1-1 and RX1-3) Turbojet Engines with Integrated Electronic Control. NACA RM E51E08, 1952.

5. Delio, G. J.; and Stiglic, P. M.: Experimental Investigation of Control Signals and the Nature of Stall and Surge Behavior in a Turbojet Engine. NACA RM E54I15, 1954.

6. Otto, Edward W.; Gold, Harold; and Hiller, Kirby W.: Design and Performance of Throttle-Type Fuel Controls for Engine Dynamic Studies. NACA TN 3445, 1955.

7. Batterton, Peter G.; and Zeller, John R.: Dynamic Performance Analysis of a Fuel-Control Valve for Use in Airbreathing Engine Research. NASA TN D-5331, 1969.

8. Zeller, John R.: Analysis of Dynamic Performance Limitations of Fast Response (150 to 200 Hz) Electrohydraulic Servos. NASA TN D-5388, 1969.

9. Zeller, John R.: Design and Analysis of a Modular Servoamplifier for Fast-Response Electrohydraulic Control Systems. NASA TN D-4898, 1968.

10. Drain, Daniel I.; Bruton, William M.; and Paulovich, Francis J.: Airbreathing Propulsion System Testing Using Sweep Frequency Techniques. NASA TN D-5485, 1969.

11. Wenzel, Leon M.; and Szuch, John R.: Analysis of Chugging in Liquid-Bipropellant Rocket Engines Using Propellants with Different Vaporization Rates. NASA TN D-3080, 1965.

12. Ketchum, J. R.; and Craig, R. T.: Simulation of Linearized Dynamics of Gas-Turbine Engines. NACA TN 2826, 1952.

13. Anon.: Computer Program for the Analysis of Annular Combustors. Vol. 1: Calculation Procedures. Rep 1111-1, Northern Research and Engineering Corp. (NASA CR-72374), Jan. 28, 1968.

NASA-Langley, 1970 —— 28 E-5595